Neural Correlates of Serial Dependence: Synaptic Short-term Plasticity Orchestrates Repulsion and Attraction

Xiuning Zhang[1]
xiuning_zhang@outlook.com

Xincheng Lu[1]
lvxc24@mails.tsinghua.edu.cn

Nihong Chen[2]*
nihongch@m.scnu.edu.cn

Yuanyuan Mi[1]*
miyuanyuan@tsinghua.edu.cn

Abstract

Serial dependence reflects how recent sensory history shapes current perception, producing two opposing biases: repulsion, where perception is repelled from recent stimuli, and attraction, where perception is drawn toward them. Repulsion typically occurs at the sensory perception stage, while attraction arises at the post-perception stage. To uncover the neural basis of these effects, we developed a two-layer continuous attractor neural network model incorporating synaptic short-term plasticity (STP). The lower layer, dominated by synaptic depression, models sensory processing and drives repulsion due to sustained neurotransmitter depletion. The higher layer, dominated by synaptic facilitation, models post-perception processing and drives attraction by sustained high neurotransmitter release probability. Our model successfully explains the serial dependence phenomena observed in the visual orientation judgment experiments, highlighting STP as the critical mechanism, with its time constants defining the temporal windows of repulsion and attraction. Furthermore, the model provides a neural foundation for the Bayesian interpretation of serial dependence. This study advances our understanding of how the neural system leverages STP to balance sensitivity in sensory perception with stability in post-perceptual cognition.

1 Introduction

The visual world casts dynamic images on the retina. From moment to moment, internal and external noise fluctuates across changes in lighting, occlusion, and viewpoint in the environment. Yet we perceive coherence and stability in the world. Serial dependence is an intrinsic mechanism through which our visual system exploits temporal correlations and contextual redundancies by merging similar stimuli that slightly change over time. The visual system harnesses this autocorrelation by inducing positive serial dependencies, drawing the current perception towards the recent history. Through continuous serial dependencies, cognition compensates for variability in sensory input, stabilizing what would otherwise be a noisy and discontinuous experience of the world [1, 2, 3, 4].

In contrast to the positive serial dependence, negative dependence is widely documented. Examples of negative serial dependence are well-known phenomena of visual adaptation and aftereffects [5, 6], e.g., a vertical grating appears to tilt clockwise after exposure to counterclockwise orientations. Such

*Corresponding authors. [1]Department of Psychological and Cognitive Sciences, Tsinghua University, Beijing 100084, China. [2]Key Laboratory of Brain, Cognition and Education Sciences, Ministry of Education; School of Psychology, Center for Studies of Psychological Application; Guangdong Key Laboratory of Mental Health and Cognitive Science, Philosophy and Social Science Laboratory of Reading and Development in Children and Adolescents; South China Normal University, Guangzhou 510631, China.

39th Conference on Neural Information Processing Systems (NeurIPS 2025).

repulsive biases have been observed in sensory cortex, as a classical behavioral probe for neural encoding of visual features [7, 8], such as orientation [9, 10], motion [11], and face viewpoint [12].

Given the coexistence of attractive and repulsive biases, the issue has been raised about the stage at which the two types of serial dependence originate. There has been growing evidence suggesting that repulsion typically occurs in the sensory stage, while attraction appears in the post-perception stage [13, 14, 15, 16, 17].

This study investigates how the cascade of neural processes is calibrated to the history of sensory and decisional events in neural networks, leveraging the unique characteristics of short-term synaptic plasticity (STP) [24, 25, 26, 27, 28, 29], wherein synaptic efficacy varies dynamically with presynaptic activity. Two competing effects exist: short-term facilitation (STF) and short-term depression (STD). Previous studies have demonstrated that STP can regulate neural information processing effectively [30, 31, 32]. For instance, STD can reduce output correlation by inhibiting high-frequency inputs, thereby reducing the autocorrelation of temporal sequences [33]; STF can facilitate the maintenance of input information by strengthening neuronal connections, thereby promoting the integration of temporal sequences [29]. Postsynaptic neurons receiving STD-dominated or STF-dominated synaptic inputs exhibit low-pass or high-pass filtering responses, respectively, achieving diversified processing of temporal sequences [34]. We hypothesize that STP underpins the neural basis of serial dependence, orchestrating its dynamic perceptual effects.

In this work, we develop a two-layer network model incorporating STP to elucidate the underlying mechanisms for both the attractive and repulsive effects in serial dependence. Specifically, to model the visual orientation judgment experiment, we adopt continuous attractor neural networks (CANNs) for each layer [35, 36]. The lower layer, characterized by STD-dominance, models sensory processing, which produces repulsion via sustained neurotransmitter depletion. The higher layer, characterized by STF-dominance, models post-perception processing, which produces attraction via sustained high neurotransmitter release probability. Our model successfully explains the serial dependence phenomena observed in experiments, revealing that the STP time constants determine the temporal windows of repulsion and attraction. Additionally, our model provides a neural mechanistic explanation of the Bayesian interpretation of serial dependence.

Related Works Contemporary models of serial dependence employ efficient encoding and Bayesian decoding to explain perceptual biases [13, 15, 18, 19, 20, 21]. In the encoding phase, prior stimuli recalibrate neural sensitivity, reshaping the probability distribution of the current stimulus to induce repulsive bias. In the decoding phase, Bayesian inference integrates sensory likelihood with a prior, yielding the posterior perception and producing attractive or repulsive biases toward prior stimuli. However, the neural basis of this dual process lacks biological validation, and the underlying circuitry dynamics remain largely unexplored. Moreover, existing models fail to capture the temporal dynamics of serial dependence, such as bias reduction with longer inter-stimulus intervals (ISI). Bridging the Bayesian framework with a mechanistic neural model remains a challenge. Recent neuroimaging advances have spurred exploration of the neural computations underlying serial dependence. Some studies attribute attraction to short-term facilitation (STF) or slow excitatory NMDA currents in higher cortical regions, with enhanced synaptic efficacy or neuronal activity [22, 23]. However, these neural dynamic models cannot explain the repulsion effect and the dynamic balance between attraction and repulsion observed in experiments.

2 The Network Model

To unveil the neural mechanism underlying serial dependence, we developed a two-layer neural network with hetero-synaptic STP. Specifically, to model visual orientation processing, we adopted a continuous attractor neural network (CANN) for each layer (Fig. 1A). CANNs are a canonical model for neural information representation [37, 38, 39], which effectively mimics the encoding of continuous features in local circuits, such as visual orientation [40, 41] and spatial location [42, 43, 44]. In the brain, stimulus information propagates from lower to higher cortical areas, establishing hierarchical processing from sensory perception to post-perceptual cognition. STP (Fig. 1B-C) is a fundamental neurophysiological property that dynamically modulates synaptic efficacy based on presynaptic firing history [45, 46], manifesting as either STF or STD. Electrophysiological studies suggest potential distinct regional specialization: sensory cortex exhibit STD-dominance [47, 48, 49, 50], while high-level cortex such as prefrontal cortex (PFC) exhibit STF-dominance [24, 53].

Therefore, the lower layer models STD-dominated processing in the visual cortex (e.g., V1), while the higher layer models STF-dominated processing in high-level cortex (e.g., PFC).

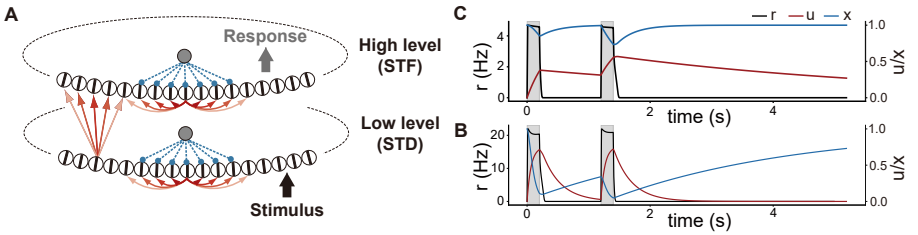

Figure 1: A two-layer CANN with heterosynaptic STP. (A) Schematic of the network model. The hierarchical two-layer architecture mimics STD-dominated processing in the visual cortex and STF-dominated processing in the higher post-perceptual cortex. Excitatory neurons within each layer are aligned in a one-dimensional ring according to their preferred orientation θ, subject to global inhibition (gray solid circle). Intra-layer and inter-layer neurons are connected with color-scaled lines that denote synaptic connectivity strength. (B) An STD-dominated network displays adaptive synaptic efficacy that sustains at low levels. During stimulation (shaded period), neural activity (r) increases the neurotransmitter release probability (u) while depleting the available neurotransmitter concentration (x). Following stimulus offset, u and x recover to baselines. (C) An STF-dominated network retains elevated synaptic efficacy (large value of u) for prolonged time.

In each layer of the CANN, neurons are aligned on a one-dimensional ring according to their preferred visual orientations $\theta \in (-\pi/2, +\pi/2]$ (Fig. 1A). Denote $h_M(\theta_M, t)$ the synaptic current to neurons at θ_M at time t, where $M = \{L, H\}$ indexes the lower (L) or higher (H) layer, and $r_M(\theta_M, t)$ the corresponding firing rate. The neuronal dynamics are described as:

$$\tau_L \frac{\partial h_L(\theta_L,t)}{\partial t} = -h_L(\theta_L,t) + \rho \int J_{LL}(\theta_L,\theta'_L) u_L(\theta'_L,t) x_L(\theta'_L,t) r_L(\theta'_L,t) d\theta'_L + I_{ext}(\theta_L,t) + \mu_L \xi_b(\theta_L,t), \tag{1}$$

$$\tau_H \frac{\partial h_H(\theta_H,t)}{\partial t} = -h_H(\theta_H,t) + \rho \int J_{HH}(\theta_H,\theta'_H) u_H(\theta'_H,t) x_H(\theta'_H,t) r_H(\theta'_H,t) d\theta'_H + \int J_{HL}(\theta_H,\theta'_L) r_L(\theta'_L,t) d\theta'_L + \mu_H \xi_b(\theta_H,t), \tag{2}$$

where τ_M, with $M = \{L, H\}$, denotes the time constant of neurons in the lower or higher layer, respectively. ρ is the neuronal density. $\xi_b(\theta_M, t)$ denotes background Gaussian white noises of zero mean and unit variance, and μ_M the noise strength. The firing rate of neurons is calculated by, $r_M(\theta_M,t) = h_M^2(\theta_M,t) / \left[1 + k_M \rho \int h_M^2(\theta'_M,t) d\theta'_M\right]$, with the parameter k_M controlling the divisive normalization strength [39]. We set the neuronal connections in the same layer or between layers to be $J_{KM}(\theta_K,\theta'_M) = J^0_{KM}/(\sqrt{2\pi}a_{KM}) \exp\left[-(\theta_K - \theta'_M)^2/(2a^2_{KM})\right]$, with $K, M \in \{L, H\}$), where J^0_{KM} denotes the maximum strengths for intra-layer connections (J^0_{LL}, J^0_{HH}) and inter-layer connections (J^0_{HL}), and a_{KM} controls the neuronal interaction range. Importantly, J_{KM} depends only on the difference $(\theta_K - \theta'_M)$, which is translation-invariant in the feature space, a crucial property enabling a CANN to maintain a continuum of attractors to represent a continuous feature [39, 51, 52].

STP modulates the synaptic efficiency between neurons, which is characterized by two variables, the neurotransmitter release probability u and the available neurotransmitter resource x. When a presynaptic neuron fires, the calcium accumulation at its axon terminal triggers two competing processes: 1) STF, due to the increase of neurotransmitter release probability u and 2) STD, due to depletion of x. The instantaneous synaptic efficacy is ux. The dynamics of STP are given by:

$$\frac{\partial u_M(\theta_M,t)}{\partial t} = -\frac{u_M(\theta_M,t)}{\tau_f^M} + U_0^M (1 - u_M(\theta_M,t)) r_M(\theta_M,t), \quad M = L, H \tag{3}$$

$$\frac{\partial x_M(\theta_M,t)}{\partial t} = \frac{1 - x_M(\theta_M,t)}{\tau_d^M} + u_M(\theta_M,t) x_M(\theta_M,t) r_M(\theta_M,t), \quad M = L, H \tag{4}$$

where the time constants τ_f and τ_d determine how quickly u and x recover to baselines, respectively. Since a larger τ_f implies that u remains at high-level after neuronal response for a longer time, it

corresponds to the STF effect; while a larger τ_d implies that x remains at low-level for a longer time, it corresponds to the STD effect. Experimental data show that sensory cortices like V1 are STD-dominated, i.e., $\tau_d \gg \tau_f$ [47], while higher cortical regions such as PFC are STF-dominated, i.e., $\tau_f \gg \tau_d$ [24, 53]. We set STP parameters in the lower and higher layers of our model accordingly (Fig. 1B-C), and the time constants also match the timescales of working memory [29, 31].

3 STP Induces Repulsion and Attraction in a Single-Layer CANN

Before studying the performance of the two-layer network, we first explore how STP induces serial-dependent biases in a single-layer CANN.

To compare the network performance with experimental data, we adopted the post-cueing adjustment paradigm (Fig. 2) [54, 55, 56, 57], where participants viewed two sequentially presented visual stimuli S_1 and S_2, whose orientations θ_1^s and θ_2^s are randomly sampled in the range of $(-\pi/2, \pi/2]$ in each trial. After a delay period, participants reported the memorized orientation, denoted as θ_{cue}^d, giving the cuing signal (Fig. 2A, D top). External visual stimuli and the cueing signal are presented to the lower layer, denoted as $I_{\text{ext}}(\theta_L, t)$, with ext $\in \{\text{sti}, \text{cue}\}$, which are expressed as $I_{\text{ext}}(\theta_L, t) = \alpha_{\text{ext}} \exp\left[-(\theta_L - \theta_{\text{ext}})^2/(2a_{\text{ext}}^2)\right] + \mu_{\text{ext}}\xi_{\text{ext}}(\theta_L, t)$, with α_{ext} controlling the signal strength, a_{ext} the signal width (inversely related to the precision), and μ_{ext} the noise strength. In the retrieval phase, we modeled the cueing signal as a weak and ambiguous copy of the corresponding stimulus signal by setting the parameters $\alpha_{\text{cue}} \ll \alpha_{\text{sti}}$, $a_{\text{cue}} > a_{\text{sti}}$, and $\mu_{\text{cue}} > \mu_{\text{sti}}$ [32], with detailed noise settings in Appendix A. We manipulated the variables, including the inter-stimulus interval (ISI, Δt_{ISI}) and the inter-trial interval (ITI, Δt_{ITI}), and measured the adjustment error of the model, which is given by Error $= \theta_2^d - \theta_2^s$, and compared it to the stimulus orientation difference $\Delta S = \theta_1^s - \theta_2^s$.

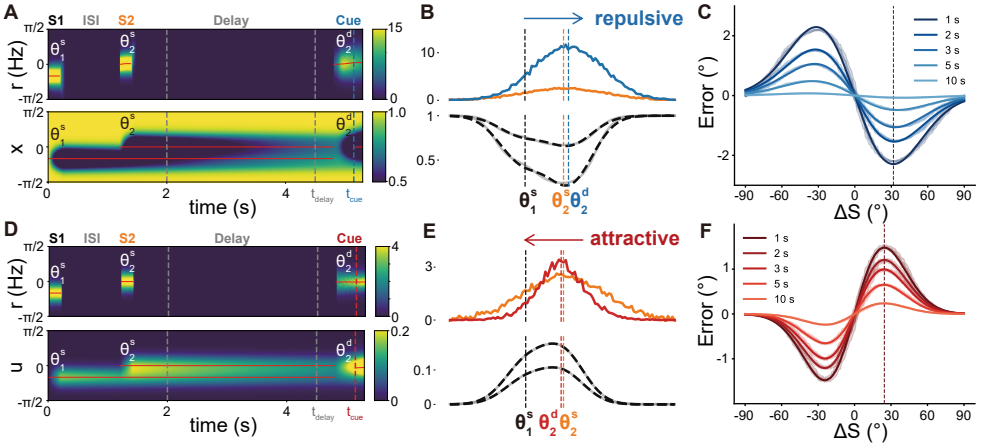

Figure 2: Serial dependence in a single-layer CANN with STP. (A-C) Repulsion effect induced by STD-dominance. (D-F) Attraction effect induced by STF-dominance. (A, D) Schematic illustration of the temporal dynamics of neural responses r, the available neurotransmitter resource x, and the neurotransmitter release probability u in a single-layer CANN with STD-dominance (A) or STF-dominance (D). Two stimuli S_1 and S_2 with respective orientations $\theta_1^s = -30°$ and $\theta_2^s = 0°$ are presented sequentially. A cueing signal is presented after the delay period to trigger the retrieval of S_2. (Top) The red line marks the decoded stimulus orientation. (Bottom) The red lines during stimulus/delay periods denote stimulus orientations in current trial. The recall-period red line indicates the recalled orientation of the second stimulus. (B, E) Illustration of the repulsive and attractive biases. In the STD-dominated case (B), the retrieved neural response (θ_2^d, blue curve) is repelled away from the earlier presented stimulus (θ_1^s). In the STF-dominated case (E), the retrieved neural response is attracted toward θ_1^s. These biased effects exist in both the neural response (top) and in the neurotransmitter concentration (bottom). Gray and dotted curves represent simulation and fitting results, respectively. (C, F) Adjustment error (Error $= \theta_2^d - \theta_2^s$) as a function of the difference between two stimuli ($\Delta S = \theta_1^s - \theta_2^s$) under different ISI conditions. It displays negative correlations (repulsion) in the STD-dominated case (C) and positive correlations (attraction) in the STF-dominated case. The shaded area represents standard error across simulation runs. For more details, see Appendix A.

3.1 STD-dominance induces repulsion in a single-layer CANN

We first demonstrated that a single-layer CANN with STD-dominance induces serial-dependent repulsion. In each trial, stimuli S_1 and S_2 activate neurons sequentially in the form of bump-shaped activities centered at θ_1^s and θ_2^s, respectively (Fig. 2A top), which deplete synaptic resources of active neurons (Fig. 2A bottom) and reduce their synaptic efficacy. The neurotransmitter concentration $x(\theta, t)$ depleted by S_1 and S_2 forms a double-trough distribution with minima at θ_1^s and θ_2^s (red curves in Fig. 2A bottom). The late presentation of S_2 implies the late recovery of corresponding neurotransmitters, resulting in $x(\theta_2^s, t) < x(\theta_1^s, t)$ (gray curve in Fig. 2B, bottom). Due to the time constants $\tau_d \gg \tau_f$, neurotransmitter concentration remains at low levels during the maintenance period, and they can be mathematically expressed as, $x(\theta, t) = 1 - A_x^1(t) \exp\left[-(\theta - \theta_1^s)^2/2a^2\right] - A_x^2(t) \exp\left[-(\theta - \theta_2^s)^2/2a^2\right]$, validated by our numerical simulation (dotted gray curve in Fig. 2B, Appendix C; the variation of $u(\theta, t)$ and $u(\theta, t)x(\theta, t)$ over time, see Appendix D). When the retrieval cue for S_2 is presented, the network generates a response bump (blue curve in Fig. 2B, top) centered at θ_2^d (decoded via population vector from neural activity, Appendix A). Notably, before presenting the retrieval cue, the double-trough distribution of $x(\theta, t)$ is lower on the side of θ_2^s closer to θ_1^s, resulting in weaker synaptic connections in this region. This creates asymmetric neuron interactions, pushing the network response θ_2^d away from θ_1^s, manifesting the repulsion effect (Fig. 2B).

We conducted 20 simulation runs (100 trials each, cue $= 2$ as examples), modeling behaviors of different participants (Appendix A). Analysis using Derivative of Gaussian function (DoG, $G(x) = \sqrt{e}(x/\sigma)A_{\text{DoG}} \exp(-x^2/2\sigma^2)$, with A_{DoG} denoting the curve's amplitude, Fig. 2C) revealed a negative correlation between the stimulus similarity ΔS and the adjustment error Error (one-sample t-test against zero on the sum of error: t(19) = 197.36, p < .001). Stimuli with higher similarity (smaller ΔS) generate stronger repulsion (larger $|\theta_2^d - \theta_2^s|$). We found that the amplitude $A_{\text{DoG}} = -2.29°$and the repulsion effect peaks at $\Delta S = 31.71°$, in agreement with the V1 repulsion observed in psychophysical experiments[15, 16, 17]. To test generality, we re-ran the one-layer model by randomly cueing S_1 or S_2 in interleaved trials. The results showed that the adjustment error curve aligns with that in Fig. 2C, with a magnitude of -3.51° (t(19) = 168.57, p < .001, Appendix E).

By manipulating ISI, we further investigated the regulation of STD on the repulsion effect, and found that: when $\Delta t_{\text{ISI}} < \tau_d$, decreasing Δt_{ISI} increases the repulsion effect (all t(19) > 43.18, p < .001). Conversely, if neurotransmitters are sufficiently recovered, the repulsion is reduced significantly.

3.2 STF-dominance induces attraction in a single-layer CANN

We continued to explore how STF affects serial dependent biases in a single-layer CANN. As shown in Fig. 2D, two sequentially presented stimuli S_1 and S_2 trigger neural activity bumps centered at θ_1^s and θ_2^s, respectively, causing the increase of neurotransmitter release probability of active neurons, and so do the interactions between them. Since the neural activity bumps caused by two stimuli are superimposed, creating a bimodal distribution of $u(\theta, t)$ peaked at θ_1^s and θ_2^s. The latter-presented S_2 induces a slower decay of the corresponding neurotransmitter release probabilities, resulting in $u(\theta_2^s, t) > u(\theta_1^s, t)$. Since the time constant of STP $\tau_f \gg \tau_d$, the neurotransmitter release probabilities remain at high levels during the maintenance period, which can be mathematically expressed as $u(\theta, t) = A_u^1(t) \exp\left[-(\theta - \theta_1^s)^2/2a^2\right] + A_u^2(t) \exp\left[-(\theta - \theta_2^s)^2/2a^2\right]$, validated by numerical simulation (dotted gray curve in Fig. 2E bottom, Appendix C; the variations of $x(\theta, t)$ and $u(\theta, t)x(\theta, t)$ over time see Appendix D). During the retrieval phase (cue $= 2$ as examples), the neurotransmitter release probabilities near θ_2^s on the side closer to θ_1^s have larger values than those on the side away from θ_1^s, causing stronger neuronal interactions in this region. Consequently, this shifts the network response center θ_2^d triggered by the cueing signal towards θ_1^s, manifesting the attraction effect (Fig. 2E top). We found that the adjustment error (Error) correlates positively with the stimulus similarity (t(19) = 122.92, p < .001), with a DoG amplitude $A_{\text{DoG}} = 1.48°$, peaking at a $\Delta S = 24.52°$(Fig. 2F), which is in agreement with the attraction effect observed in PFC and other higher cortical areas[17, 60, 61]. When randomly cueing S_1 or S_2, the adjustment error curve aligns with that in Fig. 2F, with a magnitude of 1.68° (t(19) = 96.97, p < .001, Appendix E).

By varying ISI (Fig. 2F), we found that the attraction effect (A_{DoG}) increases as Δt_{ISI} decreases, under the condition $\Delta t_{\text{ISI}} < \tau_f$ (all t(19) > 85.63, p < .001). Conversely, when neurotransmitter release probabilities decay to the baseline, the attraction effect is reduced significantly.

4 STP Orchestrates Repulsion and Attraction in a Two-layer Network

4.1 Reproducing perceptual biases in a visual orientation judgment task

Using the post-cueing paradigm, we further demonstrated that heterosynaptic STP in two layers of the model induces repulsive and attractive effects, respectively. We carried out 20 runs, each containing 100 consecutive trials. Let us consider the $(n+1)$th trial (Fig. 3A), two visual stimuli S_i^{n+1}, with orientation $\theta_i^{s,n+1}$, for $i = 1, 2$, are presented to the lower layer of the network sequentially, which trigger neuronal responses in the bump-shape centered at $\theta_{i,M}^{s,n+1}$ $(M = L, H)$, respectively, in each layer. We implemented a recall paradigm, in which a randomly selected stimulus serves as the recall cue ($S_{\text{cue}}^{s,n+1}$, cue $= \{1, 2\}$) and triggers a retrieved bump activity centered at $\theta_{\text{cue},M}^{d,n+1}$. We then calculated the adjustment errors (Error $= \theta_{\text{cue},H}^{d,n+1} - \theta_{\text{cue}}^{s,n+1}$) for cued stimuli and their relationship to both the orientation difference in the current ($\Delta S_{\text{within}} = \theta_{\text{uncue}}^{s,n+1} - \theta_{\text{cue}}^{s,n+1}$, **within-trial**) and the orientation difference cued in the preceding trial ($\Delta S_{\text{between}} = \theta_{\text{cue}}^{s,n} - \theta_{\text{cue}}^{s,n+1}$, **between-trial**).

Within-trial repulsion. According to the study in Sec. 3.1, in the lower-layer CANN with STD-dominance (modeling information processing in V1), $\theta_{\text{cue},L}^{d,n}$ in any nth trial exhibits the repulsion effect from other within-trial stimuli, as shown by the orange curve in Fig. 3B (bottom). This effect arises due to the spatially asymmetric distribution of available neurotransmitters ($x_L(\theta_L, t)$) caused by STD (gray curve). Notably, while disturbances in $x_L(\theta_L, t)$ from previous trial stimuli (S_i^{n-1}) persist, their influence is negligible because $\tau_d^L < 2T_{\text{trial}}$ (T_{trial} is the trial duration), and that $\theta_i^{s,n-1}$ and $\theta_{\text{cue},L}^{d,n-1}$ are uniformly distributed around $\theta_i^{s,n}$, making the cumulative effect statistically insignificant during the nth trial delay. The repulsively shifted neuronal responses in the lower layer are transmitted to the higher layer via feedforward connections (black curve in Fig. 3B top). Different from the lower layer, because of STF-dominance, the high layer has enhanced neurotransmitter release probabilities $u_H(\theta_H, t)$ in the region around the current trial stimuli (gray curve in Fig. 3B top). This enhanced synaptic efficacy selectively amplifies feedforward inputs centered at $\theta_{\text{cue},L}^{d,n}$. These repulsively shifted inputs from the low layer make the triggered neural response in the high layer exhibit repulsion (orange curve in Fig. 3B top).

Between-trial attraction. After two visual stimuli in the $(n+1)$th trial are presented, neurotransmitter release probabilities $u_H(\theta_H, t)$ in the higher layer exhibit a three-peak distribution, peaking at $\theta_1^{s,n+1}$, $\theta_2^{s,n+1}$, and $\theta_{\text{cue,H}}^{d,n}$ (Appendix C). Since $u_H(\theta_H, t)$ decays slowly in the high-layer, it maintains at a relatively high level during the delay period of the nth trial, and the neuronal activity induced by the retrieval cue in the high-layer further facilitates the neurotransmitter release probabilities around $\theta_{\text{cue},H}^{d,n}$ (Fig. 3A bottom), resulting in an amplitude hierarchy during the delay period in the $(n+1)$th trial: $A_u^{\text{cue},n}(t) \gg A_u^{1/2,n+1}(t)$ (gray curve in Fig. 3C top). This dynamic characteristic causes the neural activity induced by the recall cue in the $(n+1)$th trial to shift toward $\theta_{\text{cue},H}^{d,n}$, manifesting the attraction effect (orange curve in Fig. 3C top).

Statistical analysis shows that the model's adjustment error (Error $= \theta_{\text{cue},H}^{d,n+1} - \theta_{\text{cue}}^{s,n+1}$) negatively correlates with the within-trial stimulus similarity (ΔS_{within}), peaking at $38.13°$($A_{\text{DoG}} = -0.91°$, t(19) = 12.62, p < .001; Fig. 3D, blue curve); whereas, the network's adjustment error positively correlates with the between-trial stimulus similarity ($\Delta S_{\text{between}}$), peaking at $17.83°$($A_{\text{DoG}} = 1.18°$, t(19) = 7.94, p < .001; Fig. 3D, red curve). Notably, these two opposite effects are consistent with the repulsive and attractive biases observed in post-cue behavioral and neurophysiological experiments[58, 59, 61], and their magnitudes are comparable to the strength of classical serial dependence effects reported in the literature (e.g., $A_{\text{DoG}} = 1.17°$[14], $A_{\text{DoG}} = 1.32°$[20], $A_{\text{DoG}} = 1.59°$[59]). To account for potential readout bias due to asymmetric neural responses, we decoded high-layer activity using multiple methods (population vector method, center-of-mass, maximum likelihood, and peak decoding, Appendix F). All approaches yielded consistent results, confirming robust within-trial repulsion and between-trial attraction.

Psychophysical experiments also indicate that reporting the cued stimulus in the previous trial significantly affects the current between-trial attraction. By applying a partial no-report paradigm (see Appendix B), we found that when no report is required in the previous trial, the current target is less attracted to the previous one, and the within-trial repulsion effect increases slightly (between:

$A_{\text{DoG}} = 0.14°$, t(19) = 0.26, p = .802; within: $A_{\text{DoG}} = -1.29°$, t(19) = 9.21, p < .001; Fig. 3E), consistent with the psychophysical experimental data [1, 62]. Based on this, our model further predicts that compared to actual visual stimulus values (i.e., $\Delta S_{\text{between}} = \theta_{\text{cue}}^{s,n} - \theta_{\text{cue}}^{s,n+1}$), the retrieved stimulus contributes more to the between-trial attractive effect ($A_{\text{DoG}} = 1.28°$, t(19) = 8.9, p < .001; Fig. 3F), which is consistent with the psychophysical experimental data [20]. Thus, the between-trial attraction effect stems more from the memory representation difference (i.e., $\Delta R_{\text{between}} = \theta_{\text{cue,H}}^{d,n} - \theta_{\text{cue}}^{s,n+1}$).

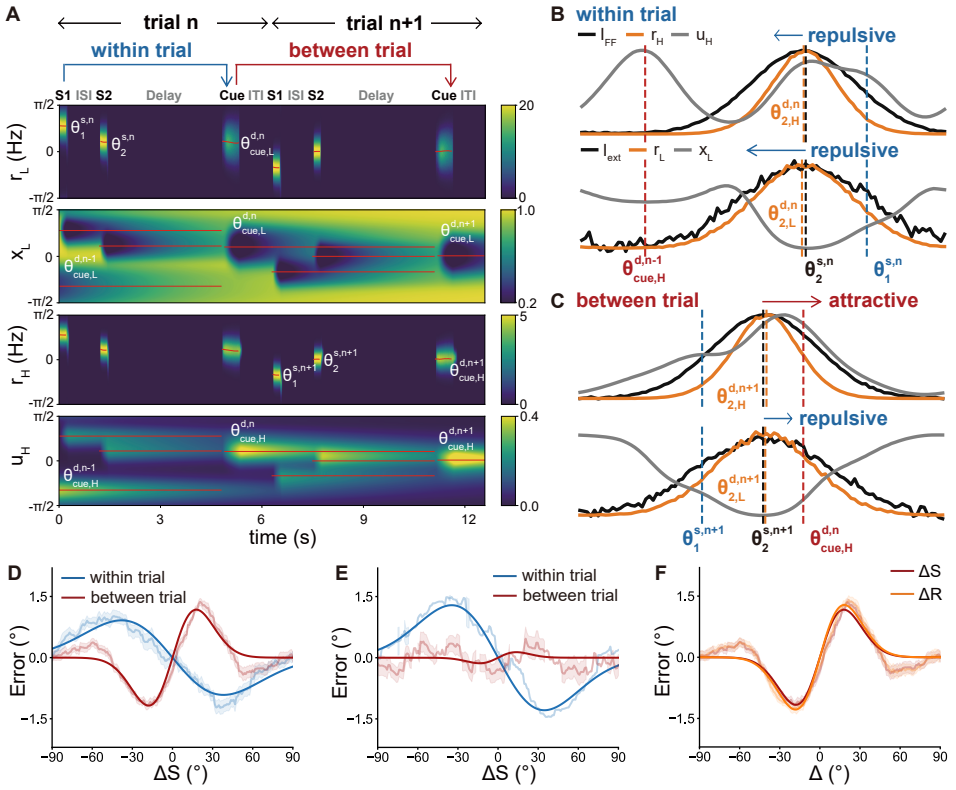

Figure 3: Serial dependence in the two-layer CANN model. (A) Temporal dynamics of the model variables. Two stimuli presented sequentially evoke neural responses. Post-delay, the network retrieves $S1$ or $S2$ based on the task cue. Plots (top to bottom): lower-layer firing rate, lower-layer available neurotransmitter resource, higher-layer firing rate, and higher-layer neurotransmitter release probability. After stimulus offset, $r_L(\theta_L)$ and $r_H(\theta_H)$ return to baseline; $x_L(\theta_L)$ and $u_H(\theta_H)$ persist, affecting decoding within and across trials. (B) Within-trial repulsion in the two-layer model. Low-layer decoded signal ($\theta_{2,L}^{d,n}$, orange curve) is biased away from the non-target ($\theta_1^{s,n}$) due to the asymmetric neurotransmitter concentration profile (gray). This propagates to the higher layer, where spatial asymmetry in $u_H(\theta_H, t)$ (gray) shifts the response bump, causing repulsion. (C) Between-trial attraction in the two-layer model. Lower-layer signal propagates to the higher layer, where $u_H(\theta_H, t)$ asymmetry (gray, top) in (n+1)th trial shifts the response bump (orange curve, top) toward $\theta_{\text{cue,H}}^{d,n}$, causing attraction. All variables normalized. (D) Within-trial repulsion and between-trial attraction. Retrieval error (angular difference between higher-layer readout and cued stimulus) plotted against the difference between the prior and current stimuli. (E) Within-trial and between-trial biases without cueing in the prior trial. (F) Within-trial and between-trial biases plotted against the difference between the prior stimulus (or its report) and the current stimulus. For more details, see Appendix B.

4.2 The neural basis of Bayesian interpretation of serial dependence

Contemporary models in the field explaining repulsion and attraction in serial dependence often adopt the Bayesian inference framework, such as the gain model [1] and two-process model [13, 20]. These models consider the whole process involving two stages (Fig. 4A): 1) sensory encoding, in which orientation-selective neurons in the sensory cortex encode stimuli in the form of tuning

curves, i.e., $r(\theta_k) = \alpha \exp[\beta \cos(\theta - \theta_k) - 1]$, with θ_k denoting the orientation preference and α, β controlling the amplitude and width of the tuning curve, respectively. 2) decision integration, in which higher cortical areas estimate stimuli through weighted integration, i.e., $\theta^d = \sum_{\theta_k} \vec{r}(\theta_k) w_k$, with w_k representing the decision weight. Although differing in regulatory strategies, both the gain and two-process models posit that the brain modulates these two processes during sequential information processing. In particular, the two-process model assumes that: 1) at the sensory encoding stage, neurons undergo adaptive sensitivity regulation, reducing tuning curve amplitudes near previous stimuli θ^s (black curves in Fig. 4A, modifying α based on $(\theta_k - \theta^s)$), which effectively alters the likelihood function in Bayesian inference; 2) at the decision stage, higher cortical areas develop weight biases toward previous stimuli (green curves in Fig. 4A, modifying w_j based on $(\theta_k - \theta^s)$), equivalent to changing the prior distribution in Bayesian inference. These dual operations shift the posterior distribution, producing repulsion in sensory perception and attraction in post-perception, but the neural basis of these operations is unknown. Also, the existing models have not explained the dynamic characteristics of serial dependence, such as the temporal decay of serial-dependent effects, the within-trial repulsion and between-trial attraction.

Our two-layer CANN model with hetero-STP provides a neural basis for the Bayesian interpretation of serial dependence, specifically, 1) negative regulation at sensory encoding: neurons responding to the presented orientation θ_i^s will experience resource depletion after activation (Fig. 4B bottom, black curve, equation see Appendix C). This reduces neuronal synaptic efficacy and affects the feedforward transmission to the higher layer, analogous to the modulation of the likelihood function in the Bayesian framework. It drives the repulsion effect as we have analyzed (Fig. 4B bottom, blue curves). 2) positive regulation at the decision stage: neurons in the higher layer responding to the previous stimulus have enhanced neurotransmitter release probabilities to the cueing orientation (Fig. 4B, green curve, Appendix C). This creates biased strong neuronal connections in the network toward the stimulus history, analogous to the modulation of the prior in the Bayesian framework. When a new stimulus arrives (the likelihood information), the high-layer CANN whose connections are implicitly modulated by the stimulus history (the prior) effectively carries out the history-dependent computation (the posterior).

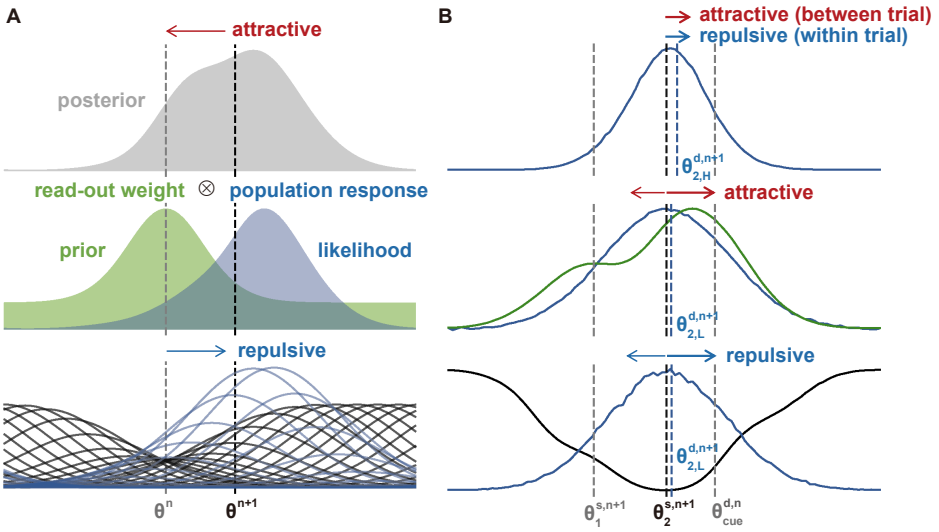

Figure 4: An STP-based Bayesian interpretation of serial dependence. (A) Schematic of Bayesian interpretation. Orientation stimuli (black curves) generate neural population responses (blue curves, likelihood), integrated by readout weights (green distributions) to produce the posterior decision. Adaptation induces repulsive effects; recent stimulus history amplifies decisional weights, eliciting attractive effects. (B) STP correlations of Bayesian inference. Bottom: neurons in the lower layer respond to the prior cued signal and current stimuli, inducing neurotransmitter depletion (gray curve). Recent stimuli evoke stronger repulsion, resulting in a net repulsive bias in the population response (blue curve). Middle: Lower-layer response (blue curve, likelihood) propagates to the higher-layer network; neurotransmitter release probability (green curve, prior) biases toward the cued target. Top: Higher-layer population response (blue curve) displays repulsive bias from the stimulus from the same trial and attractive bias toward the prior cued target.

5 Model Prediction

Within-trial repulsion effects reflect neural network sensitivity to rapid changes, while between-trial attraction effects demonstrate stability in long-term processing. In our model, these are due to the fact that STD reduces neurotransmitters, while STF increases neurotransmitter release probabilities. STP, with its time constants positioned between rapid neural encoding (hundreds of milliseconds) and experiential learning (seconds), serves as the suitable neural correlate of adaptive cognitive functions, including motor control, speech recognition, and working memory. In our two-layer network, heterogeneous STP regulates the different information processing in two layers, specifically, the lower layer employs STD for information separation, while the higher layer employs STF for information integration. This area-specific STP regulation provides a way for the neural system to balance information separation and integration, where the STP time constants determine the time boundaries for information separation and integration in temporal sequence processing.

To verify our hypothesis on the role of STP, we used the post-cueing paradigm to study the serial dependence effects by manipulating ISI and ITI time windows accordingly. We conducted 20 runs (100 trials each) for various parameter conditions. The relationship between the judgment error and the stimulus difference was fitted using a DoG curve, with amplitude (A_{DoG}) derived from this fitting (hollow circles in Fig. 5). We have two key observations: (i) When ISI within a trial is shorter than the lower layer's STD time constant (τ_d), the network shows a significant repulsion effect in judgment error (0s: $t(19) = 8.66$, $p < .001$), with its strength inversely proportional to ISI. When ISI exceeds τ_d, repulsion transitions to attraction (5s: $t(19) = 4.32$, $p < .01$; 10s: $t(19) = 5.42$, $p < .001$). Thus, the STD time constant determines the time window of repulsion, as illustrated in Fig. 5A. (ii) When ITI is shorter than the higher layer's STF time constant τ_f, the network exhibits a significant attraction effect in judgment error (all $t(19) > 4.84$, $p < .001$), with its strength inversely proportional to ITI. As ITI exceeds τ_f, the attraction effect weakens substantially and becomes negligible when ITI is sufficiently long (both $p > .05$). Thus, the STF time constant determines the time window of attraction, as shown in Fig. 5B.

The cross-talk between two layers in our model is at the neural activity level, which generates different serial dependence biases. The bottom-up repulsion competes with the STF-maintained prior information (attractive bias), yielding the observed behavioral pattern—attraction within trials and repulsion between trials. This cross-layer competition exhibits time dependency: psychophysical evidence indicates that the attractive effect is strengthened with longer delays[14], reflecting faster decay of STD-driven repulsion versus STF-sustained attraction. Our model (Fig. 5) captures this time-dependent interaction, where the short timescale of STD leads to a faster decay of repulsion, while STF in the higher layer maintains the attractive bias over longer duration.

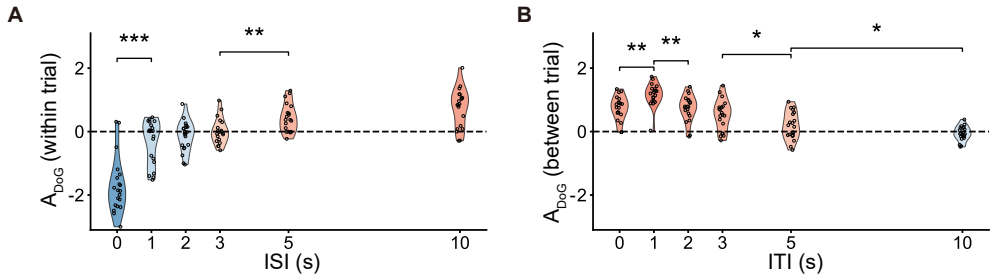

Figure 5: Model predictions on temporal windows of information segregation and integration. (A) The adjustment error (amplitude of the DoG) reveals within-trial repulsion, which gradually decreases and reverses to attraction as the ISI increases. (B) The adjustment error reveals between-trial attraction, which decreases as the ITI increases. *: $p < .05$; **: $p < .01$; ***: $p < .001$.

6 Discussion

This study proposes a hierarchical computational strategy for the neural system in dynamic sequential processing, where the STP time constants critically determine the temporal windows and boundaries for information segregation and integration. By incorporating region-specific STP heterogeneity, our continuous attractor neural networks advance the synaptic theory of working memory [29], which

posits that presynaptic neurotransmitters serve as a dynamic buffer—loaded, refreshed, and read out by spiking activity to enable both activity-based and activity-silent memory representations. In V1, STD-dominated plasticity induces a transient repulsive effect via neurotransmitter depletion, driving stimulus-specific suppression, in reminiscence of the classical visual adaptation effect [18, 47, 63, 64, 65]. In contrast, STF-dominance in PFC sustains synaptic efficacy via calcium accumulation, thereby generating attractor dynamics that support temporal integration for working memory and decision-making [29, 66, 67]. Specifically, the time constants of STD and STF dictate the temporal windows for segregation and integration, respectively, providing testable metrics for future research.

The current model resolves the apparently conflicting effects of serial dependence within a unified framework. Serial dependence, initially described as the attraction of current perception to recent stimuli, has been extended to reveal a dissociation between repulsive effects at the perceptual stage and attractive effects at post-perceptual stages [14, 15, 16, 17, 60, 61]. The neural mechanisms underlying these bidirectional biases have been widely debated, with dual-process models proposing an efficient-coding account in the sensory cortex and a decisional-inertia account in higher-order regions [13, 15, 20, 21]. The repulsive effect reflects an optimization strategy in sensory systems [19], where STD-mediated local inhibition maximizes sensitivity to stimulus changes [69]. Conversely, the attractive effect relies on STF-driven synaptic enhancement preserving historical information to enhance decoding efficiency in statistically regular environments. The order of STD and STF is crucial for the model performance. A reversed configuration—lower STF-dominated layer and higher STD-dominated layer—yielded exclusively attractive biases. Both within-trial (amplitude: 1.79°; $t(19)=6.79$, $p<.001$) and between-trial effects (amplitude: 3.81°; $t(19)=19.62$, $p<.001$; Appendix G) showed significant attraction. Reversing this order (STF-dominance first) causes initial signal smoothing due to facilitation. Consequently, even though the downstream STD layer attempts to extract differential features, the loss of sensitivity to input variation cannot be recovered, resulting in failure to achieve the intended synergy between sensitivity and stability. Sensitivity analyses confirmed that the key repulsion and attraction effects were robust to parameter variations: changing the absolute values of τ_d and τ_f (while maintaining $\tau_d \gg \tau_f$, Appendix H) or introducing ±10% random perturbations to STP parameters (Appendix I) produced only minor amplitude changes. This indicates that the results depend on the relative rather than absolute timescales, demonstrating strong model robustness.

Limitations and Future Works Our model elucidates how STP underlies Bayesian computation in biological networks. Bayesian models, such as dual-process frameworks [13, 15, 20, 21], have long been used to explain serial dependence but often lack biological substrates and fail to account for temporal dynamics. In contrast, the two-layer CANN model with hetero-STP offers a biologically grounded implementation: the likelihood function maps to STD-modulated sensory representations, the prior corresponds to STF-sustained memory traces, and their interaction yields the posterior. Unlike the conventional Bayesian models, which posit priors are shaped by long-term environmental statistics [19], the Bayesian theory of serial dependence considers experience-dependent modulations of likelihood function and prior in short timescale, and our model provides a potential neural mechanism to support this view. Since the Bayesian view of serial dependence has been recognized in the field, we hope that linking our model to this view will strengthen our understanding of the neural mechanism of serial dependence. The theoretical and mathematical foundations of this mapping require further analysis. Our model accounts for most documented serial dependence phenomena and their associated neural mechanisms, yet a few experimentally observed patterns require further investigation. For example, long-timescale repulsive effects (>50 s)[21] suggest sensory cortex mechanisms beyond current STP timescales. Implementing long-term negative feedback mechanisms in sensory cortices may explain this. In addition, future work could incorporate feedback projections to simulate top-down modulation, accounting for attractive effects observed in the sensory cortex [70]. Integrating PFC cognitive control theories could elucidate the role of higher-level attention in information processing [71, 72]. These advances will deepen our understanding of the balance between information integration and segregation, opening up new avenues in brain-inspired computing.

Acknowledgements

This work was supported by the National Science and Technology Innovation 2030 Major Program (No. 2021ZD0203700 / 2021ZD0203705, Y.Y. Mi; No. 2021ZD0203600, N.H. Chen; No. 2021ZD0204103, H. Luo), NSFC 31930053, grant from Research Center for Brain Cognition and Human Development, Guangdong, China (No. 2024B0303390003), and Science Fund for Creative Research Groups of the National Natural Science Foundation of China (T2421004). We are deeply grateful to Prof. Huan Luo and Dr. Huihui Zhang for their generous advice and insightful discussions throughout the course of this study. Their constructive feedback and encouragement have been invaluable in shaping the ideas and refining the presentation of this work.

References

[1] Fischer, J. & Whitney, D. (2014) Serial dependence in visual perception. *Nature Neuroscience* **17**, 738–743.

[2] Manassi, M., Murai, Y. & Whitney, D. (2023) Serial dependence in visual perception: A meta-analysis and review. *Journal of Vision* **23**(1), 18.

[3] Pascucci, D., Tanrikulu, Ö. D., Ozkirli, A., Houborg, C., Ceylan, G., Zerr, P., Rafiei, M. & Kristjánsson, Á. (2023) Serial dependence in visual perception: A review. *Journal of Vision* **23**(1), 9.

[4] Cicchini, G. M., Mikellidou, K. & Burr, D. C. (2024) Serial dependence in perception. *Annual Review of Psychology* **75**, 129–154.

[5] Webster, M. A., Werner, J. S. & Field, D. J. (2005) Adaptation and the phenomenology of perception. In C. W. G. Clifford & G. Rhodes (Eds.), *Fitting the Mind to the World: Adaptation and Aftereffects in High-Level Vision* (pp. 241–277). Oxford: Oxford University Press.

[6] Clifford, C. W. G., Webster, M. A., Stanley, G. B., Stocker, A. A., Kohn, A., Sharpee, T. O. & Schwartz, O. (2007) Visual adaptation: Neural, psychological and computational aspects. *Vision Research* **47**, 3125–3131.

[7] Barlow, H. (1990) A theory about the functional role and synaptic mechanism of visual aftereffects. In C. Blakemore (Ed.), *Vision: Coding and Efficiency* (pp. 597–606). Cambridge, UK: Cambridge University Press.

[8] Series, P., Stocker, A. A. & Simoncelli, E. P. (2009) Is the homunculus "aware" of sensory adaptation? *Neural Computation* **21**, 3271–3304.

[9] Gibson, J. J. & Radner, M. (1937) Adaptation, after-effect and contrast in the perception of tilted lines. I. Quantitative studies. *Journal of Experimental Psychology* **20**(5), 453–467.

[10] Müller, J. R., Metha, A. B., Krauskopf, J. & Lennie, P. (1999) Rapid adaptation in visual cortex to the structure of images. *Science* **285**(5432), 1405–1408.

[11] Levinson, E. & Sekuler, R. (1976) Adaptation alters perceived direction of motion. *Vision Research* **16**, 779–781.

[12] Fang, F. & He, S. (2005) Viewer-centered object representation in the human visual system revealed by viewpoint aftereffects. *Neuron* **45**, 793–800.

[13] Schwiedrzik, C. M., Ruff, C. C., Lazar, A., Leitner, F. C., Singer, W. & Melloni, L. (2014) Untangling perceptual memory: Hysteresis and adaptation map into separate cortical networks. *Cerebral Cortex* **24**, 1152–1164.

[14] Fritsche, M., Mostert, P. & De Lange, F. P. (2017) Opposite effects of recent history on perception and decision. *Current Biology* **27**, 590–595.

[15] Sheehan, T. C. & Serences, J. T. (2022) Attractive serial dependence overcomes repulsive neuronal adaptation. *PLOS Biology* **20**, e3001711.

[16] Hajonides, J. E., van Ede, F., Stokes, M. G., Nobre, A. C. & Myers, N. E. (2023) Multiple and dissociable effects of sensory history on working-memory performance. *Journal of Neuroscience* **43**(15), 2730–2740.

[17] Luo, M., Zhang, H., Fang, F. & Luo, H. (2025) Reactivation of previous decisions repulsively biases sensory encoding but attractively biases decision-making. *PLOS Biology* **23**, e3003150.

[18] Stocker, A. A. & Simoncelli, E. (2005) Sensory adaptation within a Bayesian framework for perception. In Y. Weiss, B. Schölkopf & J. Platt (Eds.), *Advances in Neural Information Processing Systems* (Vol. 18). Cambridge, MA: MIT Press.

[19] Wei, X. X. & Stocker, A. A. (2015) A Bayesian observer model constrained by efficient coding can explain 'anti-Bayesian' percepts. *Nature Neuroscience* **18**, 1509–1517.

[20] Pascucci, D., Mancuso, G., Santandrea, E., Della Libera, C., Plomp, G. & Chelazzi, L. (2019) Laws of concatenated perception: Vision goes for novelty, decisions for perseverance. *PLOS Biology* **17**, e3000144.

[21] Fritsche, M., Spaak, E. & De Lange, F. P. (2020) A Bayesian and efficient observer model explains concurrent attractive and repulsive history biases in visual perception. *eLife* **9**, e55389.

[22] Barbosa, J., Stein, H., Martinez, R. L., Galan-Gadea, A., Li, S., Dalmau, J., Adam, K. C. S., Valls-Solé, J., Constantinidis, C. & Compte, A. (2020) Interplay between persistent activity and activity-silent dynamics in the prefrontal cortex underlies serial biases in working memory. *Nature Neuroscience* **23**, 1016–1024.

[23] Stein, H., Barbosa, J., Rosa-Justicia, M., Prades, L., Morató, A., Galan-Gadea, A., Ariño, H., Martinez-Hernandez, E., Castro-Fornieles, J., Dalmau, J. & Compte, A. (2020) Reduced serial dependence suggests deficits in synaptic potentiation in anti-NMDAR encephalitis and schizophrenia. *Nature Communications* **11**, 4250.

[24] Markram, H. & Tsodyks, M. (1996) Redistribution of synaptic efficacy between neocortical pyramidal neurons. *Nature* **382**, 807–810.

[25] Tsodyks, M. V. & Markram, H. (1997) The neural code between neocortical pyramidal neurons depends on neurotransmitter release probability. *Proceedings of the National Academy of Sciences* **94**(2), 719–723.

[26] Markram, H., Wang, Y. & Tsodyks, M. (1998) Differential signaling via the same axon of neocortical pyramidal neurons. *Proceedings of the National Academy of Sciences* **95**, 5323–5328.

[27] Tsodyks, M., Pawelzik, K. & Markram, H. (1998) Neural networks with dynamic synapses. *Neural Computation* **10**, 821–835.

[28] Torres, J. J., Cortes, J. M., Marro, J. & Kappen, H. J. (2007) Competition between synaptic depression and facilitation in attractor neural networks. *Neural Computation* **19**(10), 2739–2755.

[29] Mongillo, G., Barak, O. & Tsodyks, M. (2008) Synaptic theory of working memory. *Science* **319**, 1543–1546.

[30] Mi, Y., Katkov, M. & Tsodyks, M. (2017) Synaptic correlates of working memory capacity. *Neuron* **93**(2), 323–330.

[31] Masse, N. Y., Yang, G. R., Song, H. F., Wang, X. J. & Freedman, D. J. (2019) Circuit mechanisms for the maintenance and manipulation of information in working memory. *Nature Neuroscience* **22**, 1159–1167.

[32] Li, J., Huang, Q., Han, Q., Mi, Y., Luo, H. & Wang, Y. (2021) Temporally coherent perturbation of neural dynamics during retention alters human multi-item working memory. *Progress in Neurobiology* **201**, 102023.

[33] Goldman, M. S., Maldonado, P. & Abbott, L. F. (2002) Redundancy reduction and sustained firing with stochastic depressing synapses. *Journal of Neuroscience* **22**(2), 584–591.

[34] Fortune, E. S. & Margoliash, D. (2001) Short-term synaptic plasticity as a temporal filter. *Trends in Neurosciences* **24**(7), 381–385.

[35] Amari, S. (1977) Dynamics of pattern formation in lateral-inhibition type neural fields. *Biological Cybernetics* **27**(2), 77–87.

[36] Zhang, K. (1996) Representation of spatial orientation by the intrinsic dynamics of the head-direction cell ensemble: A theory. *Journal of Neuroscience* **16**, 2112–2126.

[37] Ermentrout, B. (1998) Neural networks as spatio-temporal pattern-forming systems. *Reports on Progress in Physics* **61**, 353–430.

[38] Bressloff, P. C. (2012) Spatiotemporal dynamics of continuum neural fields. *Journal of Physics A: Mathematical and Theoretical* **45**(3), 033001.

[39] Wu, S., Wong, K. Y. M., Fung, C. C. A., Mi, Y. & Zhang, W. (2016) Continuous attractor neural networks: Candidate of a canonical model for neural information representation. *F1000Research* **5**(F1000 Faculty Rev), 156.

[40] Ben-Yishai, R., Bar-Or, R. L. & Sompolinsky, H. (1995) Theory of orientation tuning in visual cortex. *Proceedings of the National Academy of Sciences* **92**(9), 3844–3848.

[41] Shi, Y., Zhang, J., Li, X., Han, Y., Guan, J., Li, Y., Shen, J., Tzvetanov, T., Yang, D., Luo, X., Yao, Y., Chu, Z., Wu, T., Chen, Z., Miao, Y., Li, Y., Wang, Q., Hu, J., Meng, J., Liao, X., Zhou, Y., Tao, L., Ma, Y., Chen, J., Zhang, M., Liu, R., Mi, Y., Bao, J., Li, Z., Chen, X. & Xue, T. (2025) Non-image-forming photoreceptors improve visual orientation selectivity and image perception. *Neuron* **113**, 1–15.

[42] Samsonovich, A. & McNaughton, B. L. (1997) Path integration and cognitive mapping in a continuous attractor neural network model. *Journal of Neuroscience* **17**(15), 5900–5920.

[43] McNaughton, B. L., Battaglia, F. P., Jensen, O., Moser, E. I. & Moser, M. B. (2006) Path integration and the neural basis of the "cognitive map". *Nature Reviews Neuroscience* **7**(8), 663–678.

[44] Kim, S. S., Rouault, H., Druckmann, S. & Jayaraman, V. (2017) Ring attractor dynamics in the Drosophila central brain. *Science* **356**(6340), 849–853.

[45] Barak, O. & Tsodyks, M. (2007) Persistent activity in neural networks with dynamic synapses. *PLOS Computational Biology* **3**(2), e35.

[46] Mi, Y., Li, L., Wang, D. & Wu, S. (2014) A synaptical story of persistent activity with graded lifetime in a neural system. In *Advances in Neural Information Processing Systems* (Vol. 27, pp. 352–360).

[47] Abbott, L. F., Varela, J. A., Sen, K. & Nelson, S. B. (1997) Synaptic depression and cortical gain control. *Science* **275**, 221–224.

[48] Chung, S., Li, X. & Nelson, S. B. (2002) Short-term depression at thalamocortical synapses contributes to rapid adaptation of cortical sensory responses in vivo. *Neuron* **34**(3), 437–446.

[49] Fung, C. C. A., Wong, K. Y. M. & Wu, S. (2012) Delay compensation with dynamical synapses. In *Advances in Neural Information Processing Systems* (Vol. 25, pp. 1097–1105).

[50] Yu, Q., Bi, Z., Jiang, S., Yan, B., Chen, H., Wang, Y., Miao, Y., Li, K., Wei, Z., Xie, Y., Tan, X., Liu, X., Fu, H., Cui, L., Xing, L., Weng, S., Wang, X., Yuan, Y., Zhou, C., Wang, G., Li, L., Ma, L., Mao, Y., Chen, L. & Zhang, J. (2022) Visual cortex encodes timing information in humans and mice. *Neuron* **110**(24), 4194–4211.

[51] Zhang, W. H., Chen, A., Rasch, M. J. & Wu, S. (2016) Decentralized multisensory information integration in neural systems. *Journal of Neuroscience* **36**(2), 532–547.

[52] Yang, J., Zhang, H. & Lim, S. (2024) Sensory-memory interactions via modular structure explain errors in visual working memory. *eLife* **13**, RP95160.

[53] Wang, Y., Markram, H., Goodman, P. H., Berger, T. K., Ma, J. & Goldman-Rakic, P. S. (2006) Heterogeneity in the pyramidal network of the medial prefrontal cortex. *Nature Neuroscience* **9**, 534–542.

[54] Larocque, J. J., Lewis-Peacock, J. A., & Postle, B. R. (2014). Multiple neural states of representation in short-term memory? It's a matter of attention. *Frontiers in Human Neuroscience* **8**, 5.

[55] Christophel, T. B., Iamshchinina, P., Yan, C., Allefeld, C., Haynes, J. D. (2018). Cortical specialization for attended versus unattended working memory. *Nature Neuroscience* **21**, 494–496.

[56] Yu, Q., Teng, C., & Postle, B. R. (2020). Different states of priority recruit different neural representations in visual working memory. *PLOS Biology* **18**(6), e3000769.

[57] Huang, Q., Zhang, H., & Luo, H. (2021). Sequence structure organizes items in varied latent states of working memory neural network. *eLife* **10**, e67589.

[58] Czoschke, S., Fischer, C., Beitner, J., Kaiser, J., & Bledowski, C. (2019). Two types of serial dependence in visual working memory. *British Journal of Psychology* **110**(2), 256–267.

[59] Fischer, C., Czoschke, S., Peters, B., Rahm, B., Kaiser, J. & Bledowski, C. (2020) Context information supports serial dependence of multiple visual objects across memory episodes. *Nature Communications* **11**, 1932.

[60] Shan, J., Hajonides, J. E. & Myers, N. E. (2025) Attractive serial dependence arises during decision-making. *PLOS Biology* **23**(8), e3003333.

[61] Fischer, C., Kaiser, J. & Bledowski, C. (2025) A direct neural signature of serial dependence in working memory. *eLife* **13**, RP99478.

[62] Manassi, M., Liberman, A., Kosovicheva, A., Zhang, K. & Whitney, D. (2018) Serial dependence in position occurs at the time of perception. *Psychonomic Bulletin & Review* **25**(6), 2245–2253.

[63] Abbott, L. F., & Regehr, W. (2004) Synaptic computation. *Nature* **431**, 796–803.

[64] Reig, R., Gallego, R., Nowak, L. G. & Sánchez-Vives, M. V. (2005) Impact of cortical network activity on short-term synaptic depression. *Cerebral Cortex* **16**, 688–695.

[65] Phinney, R. E., Bowd, C. & Patterson, R. (1997) Direction-selective coding of stereoscopic (cyclopean) motion. *Vision Research* **37**(7), 865–869.

[66] Wang, X. J. (2012) Neural dynamics and circuit mechanisms of decision-making. *Current Opinion in Neurobiology* **22**(6), 1039–1046.

[67] Murray, J., Bernacchia, A., Freedman, D., Romo, R., Wallis, J., Cai, X., Padoa-Schioppa, C., Pasternak, T., Seo, H., Lee, D. & Wang, X. J. (2014) A hierarchy of intrinsic timescales across primate cortex. *Nature Neuroscience* **17**, 1661–1663.

[68] Wark, B., Lundstrom, B. N. & Fairhall, A. (2007) Sensory adaptation. *Current Opinion in Neurobiology* **17**(4), 423–429.

[69] Kohn, A. (2007) Visual adaptation: Physiology, mechanisms, and functional benefits. *Journal of Neurophysiology* **97**, 3155–3164.

[70] St. John-Saaltink, E., Kok, P., Lau, H. C., & de Lange, F. P. (2016). Serial dependence in perceptual decisions is reflected in activity patterns in primary visual cortex. *Journal of Neuroscience* **36**(23), 6186-6192.

[71] Bahmani, Z., Clark, K., Merrikhi, Y., Mueller, A., Pettine, W., Vanegas, M. I., Moore, T., & Noudoost, B. (2019). Prefrontal contributions to attention and working memory. *Current Topics in Behavioral Neurosciences* **41**, 129–153.

[72] Friedman, N. P., & Robbins, T. W. (2022). The role of prefrontal cortex in cognitive control and executive function. *Neuropsychopharmacology* **47**, 72–89.

NeurIPS Paper Checklist

1. **Claims**

   Question: Do the main claims made in the abstract and introduction accurately reflect the paper's contributions and scope?

   Answer: [Yes]

   Justification: The abstract and introduction (Sec. 1) explicitly state our key contributions and scope.

   Guidelines:

   - The answer NA means that the abstract and introduction do not include the claims made in the paper.
   - The abstract and/or introduction should clearly state the claims made, including the contributions made in the paper and important assumptions and limitations. A No or NA answer to this question will not be perceived well by the reviewers.
   - The claims made should match theoretical and experimental results, and reflect how much the results can be expected to generalize to other settings.
   - It is fine to include aspirational goals as motivation as long as it is clear that these goals are not attained by the paper.

2. **Limitations**

   Question: Does the paper discuss the limitations of the work performed by the authors?

   Answer: [Yes]

   Justification: We discussed the limitation of our work in Sec. 6(discussion).

   Guidelines:

   - The answer NA means that the paper has no limitation while the answer No means that the paper has limitations, but those are not discussed in the paper.
   - The authors are encouraged to create a separate "Limitations" section in their paper.
   - The paper should point out any strong assumptions and how robust the results are to violations of these assumptions (e.g., independence assumptions, noiseless settings, model well-specification, asymptotic approximations only holding locally). The authors should reflect on how these assumptions might be violated in practice and what the implications would be.
   - The authors should reflect on the scope of the claims made, e.g., if the approach was only tested on a few datasets or with a few runs. In general, empirical results often depend on implicit assumptions, which should be articulated.
   - The authors should reflect on the factors that influence the performance of the approach. For example, a facial recognition algorithm may perform poorly when image resolution is low or images are taken in low lighting. Or a speech-to-text system might not be used reliably to provide closed captions for online lectures because it fails to handle technical jargon.
   - The authors should discuss the computational efficiency of the proposed algorithms and how they scale with dataset size.
   - If applicable, the authors should discuss possible limitations of their approach to address problems of privacy and fairness.
   - While the authors might fear that complete honesty about limitations might be used by reviewers as grounds for rejection, a worse outcome might be that reviewers discover limitations that aren't acknowledged in the paper. The authors should use their best judgment and recognize that individual actions in favor of transparency play an important role in developing norms that preserve the integrity of the community. Reviewers will be specifically instructed to not penalize honesty concerning limitations.

3. **Theory assumptions and proofs**

   Question: For each theoretical result, does the paper provide the full set of assumptions and a complete (and correct) proof?

   Answer: [NA]

Justification: The paper does not include theoretical results.

Guidelines:

- The answer NA means that the paper does not include theoretical results.
- All the theorems, formulas, and proofs in the paper should be numbered and cross-referenced.
- All assumptions should be clearly stated or referenced in the statement of any theorems.
- The proofs can either appear in the main paper or the supplemental material, but if they appear in the supplemental material, the authors are encouraged to provide a short proof sketch to provide intuition.
- Inversely, any informal proof provided in the core of the paper should be complemented by formal proofs provided in appendix or supplemental material.
- Theorems and Lemmas that the proof relies upon should be properly referenced.

4. **Experimental result reproducibility**

   Question: Does the paper fully disclose all the information needed to reproduce the main experimental results of the paper to the extent that it affects the main claims and/or conclusions of the paper (regardless of whether the code and data are provided or not)?

   Answer: [Yes]

   Justification: We described our model in Sec. 2 and included model and experimental details in Appendix A and B.

   Guidelines:

   - The answer NA means that the paper does not include experiments.
   - If the paper includes experiments, a No answer to this question will not be perceived well by the reviewers: Making the paper reproducible is important, regardless of whether the code and data are provided or not.
   - If the contribution is a dataset and/or model, the authors should describe the steps taken to make their results reproducible or verifiable.
   - Depending on the contribution, reproducibility can be accomplished in various ways. For example, if the contribution is a novel architecture, describing the architecture fully might suffice, or if the contribution is a specific model and empirical evaluation, it may be necessary to either make it possible for others to replicate the model with the same dataset, or provide access to the model. In general. releasing code and data is often one good way to accomplish this, but reproducibility can also be provided via detailed instructions for how to replicate the results, access to a hosted model (e.g., in the case of a large language model), releasing of a model checkpoint, or other means that are appropriate to the research performed.
   - While NeurIPS does not require releasing code, the conference does require all submissions to provide some reasonable avenue for reproducibility, which may depend on the nature of the contribution. For example
     (a) If the contribution is primarily a new algorithm, the paper should make it clear how to reproduce that algorithm.
     (b) If the contribution is primarily a new model architecture, the paper should describe the architecture clearly and fully.
     (c) If the contribution is a new model (e.g., a large language model), then there should either be a way to access this model for reproducing the results or a way to reproduce the model (e.g., with an open-source dataset or instructions for how to construct the dataset).
     (d) We recognize that reproducibility may be tricky in some cases, in which case authors are welcome to describe the particular way they provide for reproducibility. In the case of closed-source models, it may be that access to the model is limited in some way (e.g., to registered users), but it should be possible for other researchers to have some path to reproducing or verifying the results.

5. **Open access to data and code**

   Question: Does the paper provide open access to the data and code, with sufficient instructions to faithfully reproduce the main experimental results, as described in supplemental material?

Answer: [No]

Justification: The code is currently under internal review and cannot be released at this time, but model and experimental details are documented in Appendix A and B for reproduction.

Guidelines:

- The answer NA means that paper does not include experiments requiring code.
- Please see the NeurIPS code and data submission guidelines (`https://nips.cc/public/guides/CodeSubmissionPolicy`) for more details.
- While we encourage the release of code and data, we understand that this might not be possible, so "No" is an acceptable answer. Papers cannot be rejected simply for not including code, unless this is central to the contribution (e.g., for a new open-source benchmark).
- The instructions should contain the exact command and environment needed to run to reproduce the results. See the NeurIPS code and data submission guidelines (`https://nips.cc/public/guides/CodeSubmissionPolicy`) for more details.
- The authors should provide instructions on data access and preparation, including how to access the raw data, preprocessed data, intermediate data, and generated data, etc.
- The authors should provide scripts to reproduce all experimental results for the new proposed method and baselines. If only a subset of experiments are reproducible, they should state which ones are omitted from the script and why.
- At submission time, to preserve anonymity, the authors should release anonymized versions (if applicable).
- Providing as much information as possible in supplemental material (appended to the paper) is recommended, but including URLs to data and code is permitted.

6. **Experimental setting/details**

   Question: Does the paper specify all the training and test details (e.g., data splits, hyperparameters, how they were chosen, type of optimizer, etc.) necessary to understand the results?

   Answer: [Yes]

   Justification: Detailed methods including training and test details can be found in Appendix A and B.

   Guidelines:

   - The answer NA means that the paper does not include experiments.
   - The experimental setting should be presented in the core of the paper to a level of detail that is necessary to appreciate the results and make sense of them.
   - The full details can be provided either with the code, in appendix, or as supplemental material.

7. **Experiment statistical significance**

   Question: Does the paper report error bars suitably and correctly defined or other appropriate information about the statistical significance of the experiments?

   Answer: [Yes]

   Justification: We calculated 20 runs for each experiment. We reported standard error in Fig. 2 and 3 and the statistical significance in Fig. 5.

   Guidelines:

   - The answer NA means that the paper does not include experiments.
   - The authors should answer "Yes" if the results are accompanied by error bars, confidence intervals, or statistical significance tests, at least for the experiments that support the main claims of the paper.
   - The factors of variability that the error bars are capturing should be clearly stated (for example, train/test split, initialization, random drawing of some parameter, or overall run with given experimental conditions).
   - The method for calculating the error bars should be explained (closed form formula, call to a library function, bootstrap, etc.)

- The assumptions made should be given (e.g., Normally distributed errors).
- It should be clear whether the error bar is the standard deviation or the standard error of the mean.
- It is OK to report 1-sigma error bars, but one should state it. The authors should preferably report a 2-sigma error bar than state that they have a 96% CI, if the hypothesis of Normality of errors is not verified.
- For asymmetric distributions, the authors should be careful not to show in tables or figures symmetric error bars that would yield results that are out of range (e.g. negative error rates).
- If error bars are reported in tables or plots, The authors should explain in the text how they were calculated and reference the corresponding figures or tables in the text.

8. **Experiments compute resources**

   Question: For each experiment, does the paper provide sufficient information on the computer resources (type of compute workers, memory, time of execution) needed to reproduce the experiments?

   Answer: [Yes]

   Justification: All experiments were conducted on a consumer-grade desktop computer (AMD Ryzen 9 9950X, 32GB DDR5 RAM) with hour-scale runtimes.

   Guidelines:

   - The answer NA means that the paper does not include experiments.
   - The paper should indicate the type of compute workers CPU or GPU, internal cluster, or cloud provider, including relevant memory and storage.
   - The paper should provide the amount of compute required for each of the individual experimental runs as well as estimate the total compute.
   - The paper should disclose whether the full research project required more compute than the experiments reported in the paper (e.g., preliminary or failed experiments that didn't make it into the paper).

9. **Code of ethics**

   Question: Does the research conducted in the paper conform, in every respect, with the NeurIPS Code of Ethics `https://neurips.cc/public/EthicsGuidelines`?

   Answer: [Yes]

   Justification: We have read the NeurIPS Code of Ethics and made sure that the paper conforms to it.

   Guidelines:

   - The answer NA means that the authors have not reviewed the NeurIPS Code of Ethics.
   - If the authors answer No, they should explain the special circumstances that require a deviation from the Code of Ethics.
   - The authors should make sure to preserve anonymity (e.g., if there is a special consideration due to laws or regulations in their jurisdiction).

10. **Broader impacts**

    Question: Does the paper discuss both potential positive societal impacts and negative societal impacts of the work performed?

    Answer: [NA]

    Justification: This work is fundamental research and not tied to particular applications.

    Guidelines:

    - The answer NA means that there is no societal impact of the work performed.
    - If the authors answer NA or No, they should explain why their work has no societal impact or why the paper does not address societal impact.
    - Examples of negative societal impacts include potential malicious or unintended uses (e.g., disinformation, generating fake profiles, surveillance), fairness considerations (e.g., deployment of technologies that could make decisions that unfairly impact specific groups), privacy considerations, and security considerations.

- The conference expects that many papers will be foundational research and not tied to particular applications, let alone deployments. However, if there is a direct path to any negative applications, the authors should point it out. For example, it is legitimate to point out that an improvement in the quality of generative models could be used to generate deepfakes for disinformation. On the other hand, it is not needed to point out that a generic algorithm for optimizing neural networks could enable people to train models that generate Deepfakes faster.
- The authors should consider possible harms that could arise when the technology is being used as intended and functioning correctly, harms that could arise when the technology is being used as intended but gives incorrect results, and harms following from (intentional or unintentional) misuse of the technology.
- If there are negative societal impacts, the authors could also discuss possible mitigation strategies (e.g., gated release of models, providing defenses in addition to attacks, mechanisms for monitoring misuse, mechanisms to monitor how a system learns from feedback over time, improving the efficiency and accessibility of ML).

11. **Safeguards**

    Question: Does the paper describe safeguards that have been put in place for responsible release of data or models that have a high risk for misuse (e.g., pretrained language models, image generators, or scraped datasets)?

    Answer: [NA]

    Justification: The paper poses no such risks.

    Guidelines:

    - The answer NA means that the paper poses no such risks.
    - Released models that have a high risk for misuse or dual-use should be released with necessary safeguards to allow for controlled use of the model, for example by requiring that users adhere to usage guidelines or restrictions to access the model or implementing safety filters.
    - Datasets that have been scraped from the Internet could pose safety risks. The authors should describe how they avoided releasing unsafe images.
    - We recognize that providing effective safeguards is challenging, and many papers do not require this, but we encourage authors to take this into account and make a best faith effort.

12. **Licenses for existing assets**

    Question: Are the creators or original owners of assets (e.g., code, data, models), used in the paper, properly credited and are the license and terms of use explicitly mentioned and properly respected?

    Answer: [NA]

    Justification: Our work does not use existing assets.

    Guidelines:

    - The answer NA means that the paper does not use existing assets.
    - The authors should cite the original paper that produced the code package or dataset.
    - The authors should state which version of the asset is used and, if possible, include a URL.
    - The name of the license (e.g., CC-BY 4.0) should be included for each asset.
    - For scraped data from a particular source (e.g., website), the copyright and terms of service of that source should be provided.
    - If assets are released, the license, copyright information, and terms of use in the package should be provided. For popular datasets, `paperswithcode.com/datasets` has curated licenses for some datasets. Their licensing guide can help determine the license of a dataset.
    - For existing datasets that are re-packaged, both the original license and the license of the derived asset (if it has changed) should be provided.

- If this information is not available online, the authors are encouraged to reach out to the asset's creators.

13. **New assets**

    Question: Are new assets introduced in the paper well documented and is the documentation provided alongside the assets?

    Answer: [NA]

    Justification: The paper does not release new assets.

    Guidelines:

    - The answer NA means that the paper does not release new assets.
    - Researchers should communicate the details of the dataset/code/model as part of their submissions via structured templates. This includes details about training, license, limitations, etc.
    - The paper should discuss whether and how consent was obtained from people whose asset is used.
    - At submission time, remember to anonymize your assets (if applicable). You can either create an anonymized URL or include an anonymized zip file.

14. **Crowdsourcing and research with human subjects**

    Question: For crowdsourcing experiments and research with human subjects, does the paper include the full text of instructions given to participants and screenshots, if applicable, as well as details about compensation (if any)?

    Answer: [NA]

    Justification: The paper does not involve crowdsourcing nor research with human subjects.

    Guidelines:

    - The answer NA means that the paper does not involve crowdsourcing nor research with human subjects.
    - Including this information in the supplemental material is fine, but if the main contribution of the paper involves human subjects, then as much detail as possible should be included in the main paper.
    - According to the NeurIPS Code of Ethics, workers involved in data collection, curation, or other labor should be paid at least the minimum wage in the country of the data collector.

15. **Institutional review board (IRB) approvals or equivalent for research with human subjects**

    Question: Does the paper describe potential risks incurred by study participants, whether such risks were disclosed to the subjects, and whether Institutional Review Board (IRB) approvals (or an equivalent approval/review based on the requirements of your country or institution) were obtained?

    Answer: [NA]

    Justification: The paper does not involve crowdsourcing nor research with human subjects.

    Guidelines:

    - The answer NA means that the paper does not involve crowdsourcing nor research with human subjects.
    - Depending on the country in which research is conducted, IRB approval (or equivalent) may be required for any human subjects research. If you obtained IRB approval, you should clearly state this in the paper.
    - We recognize that the procedures for this may vary significantly between institutions and locations, and we expect authors to adhere to the NeurIPS Code of Ethics and the guidelines for their institution.
    - For initial submissions, do not include any information that would break anonymity (if applicable), such as the institution conducting the review.

16. **Declaration of LLM usage**

Question: Does the paper describe the usage of LLMs if it is an important, original, or non-standard component of the core methods in this research? Note that if the LLM is used only for writing, editing, or formatting purposes and does not impact the core methodology, scientific rigorousness, or originality of the research, declaration is not required.

Answer: [NA]

Justification: The core method development in this research does not involve LLMs as any important, original, or non-standard components.

Guidelines:

- The answer NA means that the core method development in this research does not involve LLMs as any important, original, or non-standard components.
- Please refer to our LLM policy (`https://neurips.cc/Conferences/2025/LLM`) for what should or should not be described.

Appendix

A Model Details

Single-layer CANN and two-layer CANN. The neural dynamics in a single-layer CANN are described as:

$$\tau \frac{\partial h(\theta,t)}{\partial t} = -h(\theta,t) + \rho \int J(\theta,\theta') u(\theta',t) x(\theta',t) r(\theta',t) d\theta' + I_{\text{ext}}(\theta,t) + \mu_b \xi_b(\theta,t) \quad (5)$$

The calculation of $u(\theta,t)$, $x(\theta,t)$, $r(\theta,t)$ was identical to the two-layer CANN in Sec. 2. The time constants for short-term depression (τ_d) and short-term facilitation (τ_f) were set for the STD-dominated CANN and the STF-dominated CANN models, respectively.

We considered heterogeneity in intra-layer and inter-layer neuronal connections across different participants by including noise: $\widetilde{J}_{KM}(\theta_K,\theta'_M) = J_{KM}(\theta_K,\theta'_M)(1+\mu_J\xi_J)$, with $K,M \in \{L,H\}$. ξ_J denotes white Gaussian noise of zero mean and unit variance and μ_J the noise strength. We included noise in the neuronal connections of the single-layer CANN similarly. Model parameters are shown in Tab. 1.

Population vector method. We decoded orientation value from neural activity across CANN layers using the population vector method, expressed as:

$$\theta^d = \frac{\int \theta \langle r(\theta,t)\rangle d\theta}{\int \langle r(\theta,t)\rangle d\theta} \quad (6)$$

where $\langle r(\theta,t)\rangle$ is the averaged firing rate of neurons at θ during the cueing period.

B Experimental Paradigm and Statistical Methods

Post-cueing paradigm. Each trial consists of a first stimulus (S_1) lasting 200 ms, an inter-stimulus interval (ISI) lasting 1000 ms, a second stimulus (S_2) lasting 200 ms, a delay period of 3400 ms, a retrieval cue ($S_i, i = 1,2$) lasting 500 ms, and an inter-trial interval (ITI) of 1000 ms. In the single-layer CANN, S_2 was recalled during the cue phase to examine the influence of S_1 on S_2 within a trial. Simulations were performed for a single trial. In the two-layer CANN, the effects within and between trials were examined by recalling S_1 or S_2 during the cue phase in a randomized order across 100 consecutive trials. Simulations were conducted with 20 participants, each with various neuronal synaptic connection strengths as in Appendix A. For each participant, 100 trials were conducted.

Stimulus orientation settings. Orientations were selected from a uniform distribution over [-90°, 90°) with a step size of 1°. ΔS refers to the angular difference between the previous stimulus and the current stimulus. To ensure an equal probability of its occurrence, ΔS_{within} and $\Delta S_{\text{between}}$ were randomly generated with equal probability over [-90°, 90°]. Take the first trial in the two-layer CANN as an example, $\theta^{s,1}_{\text{cue}}$ was selected from a uniform distribution over [-90°, 90°) randomly, then $\theta^{s,1}_{\text{uncue}}$ and $\theta^{s,2}_{\text{cue}}$ were calculated:

$$\theta^{s,1}_{\text{uncue}} = \theta^{s,1}_{\text{cue}} + \Delta S_{\text{within}} \quad (7)$$

$$\theta^{s,2}_{\text{cue}} = \theta^{s,1}_{\text{cue}} - \Delta S_{\text{between}} \quad (8)$$

Subsequent stimuli were generated in the same way. For the nth trial, $\theta^{s,n}_{\text{uncue}}$ of the current trial and $\theta^{s,n+1}_{\text{cue}}$ of the subsequent trial were calculated according to the following formulas:

$$\theta^{s,n}_{\text{uncue}} = \theta^{s,n}_{\text{cue}} + \Delta S_{\text{within}} \quad (9)$$

$$\theta^{s,n+1}_{\text{cue}} = \theta^{s,n}_{\text{cue}} - \Delta S_{\text{between}} \quad (10)$$

θ^n_{cue} and θ^n_{uncue} were assigned to S_1 or S_2 randomly, meanwhile, the cue index in S^n_{cue} was determined.

Behavioral readout. In a single-layer CANN, external signals are input into the network, and the output is read from the same network using the population vector method. In a two-layer CANN, external signals are input into the lower layer, and the output is read from the higher layer.

Table 1: Model Parameters

Parameter	Meaning	Value
General Network Parameters		
N	Number of neurons	100
τ	Time constant of synaptic current	0.01 s
μ_J	Neuronal interaction noise strength	0.01
Parameters for STD-dominated single-layer CANN (Fig. 2A-C)		
J^0	Maximum synaptic connection strength	0.13
a	Range of neuronal interaction	0.5
k	Global inhibition strength	0.0018
μ_b	Background noise strength	0.5
τ_d	Time constant of x	3 s
τ_f	Time constant of u	0.3 s
U_0	Increment of u produced by a spike	0.5
Parameters for STF-dominated single-layer CANN (Fig. 2D-F)		
J^0	Maximum synaptic connection strength	0.09
a	Range of neuronal interaction	0.15
k	Global inhibition strength	0.0095
μ_b	Background noise strength	0.5
τ_d	Time constant of x	0.3 s
τ_f	Time constant of u	5 s
U_0	Increment of u produced by a spike	0.2
Parameters for two-layer network (Fig. 3)		
J^0_{LL}	Max synaptic connection strength (low-to-low)	0.13
a_L	Range of neuronal interaction (low-level)	0.5
k_L	Global inhibition strength (low-level)	0.0018
μ_L	Background noise strength (low-level)	0.5
τ^L_d	Time constant of x (low-level)	3 s
τ^L_f	Time constant of u (low-level)	0.3 s
U^L_0	Increment of u produced by a spike (low-level)	0.5
J^0_{HL}	Max synaptic connection strength (low-to-high)	0.02
a_{HL}	Range of neuronal interaction (low-to-high)	0.15
J^0_{HH}	Max synaptic strength (high-to-high)	0.09
a_H	Range of neuronal interaction (high-level)	0.15
k_H	Global inhibition strength (high-level)	0.0095
μ_H	Background noise strength (high-level)	0.5
τ^H_d	Time constant of x (high-level)	0.3 s
τ^H_f	Time constant of u (high-level)	5 s
U^H_0	Increment of u produced by a spike (high-level)	0.2
External Input		
α_{sti}	Strength of external stimulus	20
a_{sti}	Spatial scale of external stimulus	0.3
μ_{sti}	Noise strength of external stimulus	0.5
α_{cue}	Strength of external cue	2.5
a_{cue}	Spatial scale of external cue	0.4
μ_{cue}	Noise strength of external cue	1

Adjustment error. For each trial, we measured the adjustment error as the angular distance between the cued stimulus angle and the decoded response angle.

$$\text{Error} = \theta^d_{\text{cue}} - \theta^s_{\text{cue}} \tag{11}$$

Serial bias analysis. Serial bias was calculated as the averaged adjustment error using a 30° sliding window, as a function of within-trial and between-trial angular differences. In Fig. 3D, E:

$$\Delta S_{\text{within}} = \theta^{s,n}_{\text{uncue}} - \theta^{s,n}_{\text{cue}} \tag{12}$$

$$\Delta S_{\text{between}} = \theta^{s,n}_{\text{cue}} - \theta^{s,n+1}_{\text{cue}} \tag{13}$$

In Fig. 3F, we further analyzed the average error as a function of the memory representation angular difference:

$$\Delta R_{\text{between}} = \theta^{d,n}_{\text{cue}} - \theta^{s,n+1}_{\text{cue}} \tag{14}$$

DoG curve. To measure the amplitude of serial dependence, we fit the error plot with the first derivative of a Gaussian curve (DoG) $G(x) = \sqrt{e}(x/\sigma)A_{\text{DoG}}\exp(-x^2/2\sigma^2)$, where A_{DoG} is the amplitude of the curve peak, σ is the curve width.

Partial no-report paradigm. To test whether serial dependence occurs without a prior reported stimulus, the cue was absent in 40% of the trials. Trials following those without a report were used to analyze serial biases.

Computer resources. We used Python 3.11.9 and Brainpy 2.6.0.post20240918 for simulations. All experiments were conducted on a consumer-grade desktop computer (AMD Ryzen 9 9950X, 32GB DDR5 RAM) with hour-scale runtimes.

C Numerical Simulation of u and x

The fitting of x curve in an STD-dominated single-layer CANN. In an STD-dominated single-layer CANN, x is fitted by the following equation:

$$x(\theta,t) = 1 - A^1_x(t)\exp\left[-(\theta-\theta^s_1)^2/2a^2\right] - A^2_x(t)\exp\left[-(\theta-\theta^s_2)^2/2a^2\right] \tag{15}$$

For example, in Fig. 2B, we set $\theta^s_1 = -30°$, $\theta^s_2 = 0°$ as the initial guess value. The amplitudes $A^1_x(t)$ and $A^2_x(t)$ decayed from the early delay period (Fig. S1A) to the late delay period (Fig. S1B). We calculated these parameters from the time point after S_2 disappeared (t_0 = 1.5 s) to the time point before the cue period (t_e = 4.8 s), shown as dots in Fig. S1C, and found that they decayed exponentially with a time constant τ_d (curve in Fig. S1C), described as:

$$A^i_x(t) = A^i_x(t_0)\exp\left[-(t-t_0)/\tau_d\right], i = 1,2 \tag{16}$$

where $A^1_x(t_0) = 0.46, A^2_x(t_0) = 0.68$.

The above analysis is applicable to other combinations of θ^s_1 and θ^s_2.

Table 2: The fitting parameters of x curve

t (s)	θ^s_1 (°)	θ^s_2 (°)	A^1_x	A^2_x	a
2.0	-32.72	6.13	0.39	0.57	0.31
4.5	-32.72	6.13	0.17	0.25	0.31

The fitting of u curve in an STF-dominated single-layer CANN. In an STF-dominated single-layer CANN, the u curve was fitted by the following equation:

$$u(\theta,t) = A^1_u(t)\exp\left[-(\theta-\theta^s_1)^2/2a^2\right] + A^2_u(t)\exp\left[-(\theta-\theta^s_2)^2/2a^2\right] \tag{17}$$

In Fig. 2E, we fixed $\theta^s_1 = -30°$ and $\theta^s_2 = 0°$. The amplitude parameters $A^1_u(t)$ and $A^2_u(t)$ decayed from the early delay period (Fig. S1D) to the late delay period (Fig. S1E). We calculated these parameters from the time point after S_2 disappeared (t_0 = 1.5 s) to the time point before the cue period (t_e = 4.8 s), shown as dots in Fig. S1F, and found that they decayed exponentially with the time constant τ_f (curve in Fig. S1F), described as:

$$A^i_u(t) = A^i_u(t_0)\exp\left[-(t-t_0)/\tau_f\right], i = 1,2 \tag{18}$$

where $A^1_u(t_0) = 0.09, A^2_u(t_0) = 0.12$.

The above analysis is applicable to other combinations of θ^s_1 and θ^s_2.

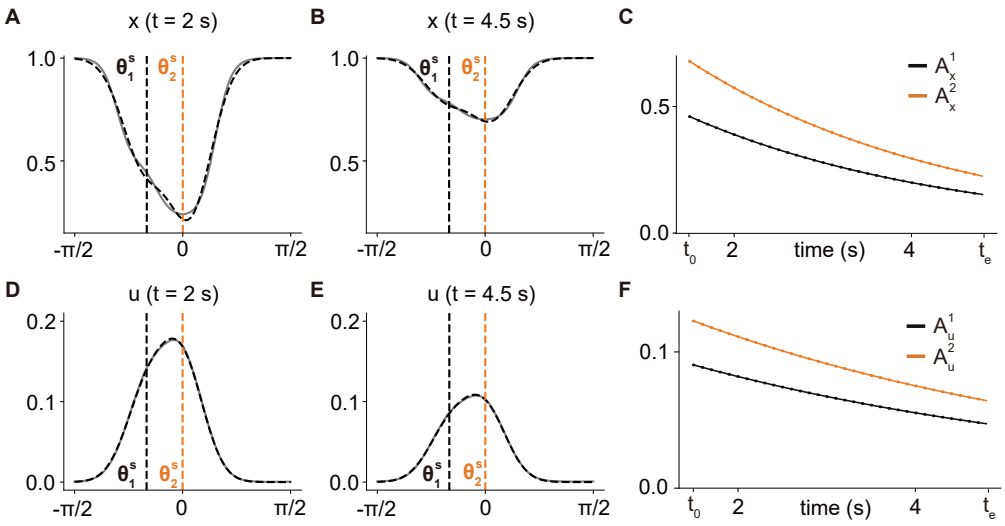

Figure S1: The fitting of x and u curves in a single-layer CANN. (A-C) x in an STD-dominated single-layer CANN. (D-F) u in an STF-dominated single-layer CANN. (A, D) Simulation (gray curve) and fitting results (dotted curve) in the early delay period (t = 2.0 s). (B, E) Simulation (gray curve) and fitting results (dotted curve) the late delay period (t = 4.5 s). (C, F) Exponential decay during the delay period. Dots represent the simulation results, and curves represent the exponential fitting results.

Table 3: The fitting parameters of u curve

t (s)	θ_1^s (°)	θ_2^s (°)	A_u^1	A_u^2	a
2.0	-30.00	0.00	0.08	0.11	0.31
4.5	-30.00	0.00	0.05	0.07	0.31

The fitting of x_L and u_H curve in a two-layer CANN. In a two-layer CANN, the x_L curve in the $(n+1)th$ trial was fitted by the following equation:

$$x_L(\theta_L,t) = 1 - A_x^1(t)\exp\left[-(\theta_L-\theta_1^{s,n+1})^2/2a_x^2\right] - A_x^2(t)\exp\left[-(\theta_L-\theta_2^{s,n+1})^2/2a_x^2\right] - A_x^{\text{cue}}(t)\exp\left[-(\theta_L-\theta_{\text{cue}}^{s,n})^2/2a_x^2\right] \quad (19)$$

In Fig. 4B, we set $\theta_{\text{cue}}^n = 20°$, $\theta_1^{n+1} = -30°$, and $\theta_2^{n+1} = 0°$ as the initial guess values. The amplitude parameters $A_x^{\text{cue}}(t)$, $A_x^1(t)$ and $A_x^2(t)$ decayed from the early delay period (Fig. S2A) to the late delay period (Fig. S2B). We calculated the fitted parameters from the time point after S_2^{n+1} disappeared (t_0 = 7.8 s) to the time point before the cue period (t_e = 11.1 s), shown as dots in Fig. S2C, and found that they decayed exponentially with a time constant of τ_d (curve in Fig. S2C), which can also be described as:

$$A_x^i(t) = A_x^i(t_0)\exp\left[-(t-t_0)/\tau_d\right], i = 1, 2, \text{cue} \quad (20)$$

where $A_x^{\text{cue}}(t_0) = 0.23, A_x^1(t_0) = 0.44, A_x^2(t_0) = 0.68$.

The above analysis is applicable to other combinations of θ_{cue}^n, θ_1^{n+1} and θ_2^{n+1}.

Table 4: The fitting parameters of x_L curve

t (s)	$\theta_{\text{cue}}^{d,n}$ (°)	$\theta_1^{s,n+1}$ (°)	$\theta_2^{s,n+1}$ (°)	A_x^{cue}	A_x^1	A_x^2	a_x
8.3	39.13	-35.41	3.26	0.19	0.37	0.57	0.33
10.8	39.13	-35.41	3.26	0.08	0.16	0.25	0.33

u_H curve in the $(n+1)th$ trial can be fit by the following equation:

$$u_H(\theta_H, t) = A_u^1(t)\exp\left[-(\theta_H - \theta_1^{s,n+1})^2/2a_u^2\right] + A_u^2(t)\exp\left[-(\theta_H - \theta_2^{s,n+1})^2/2a_u^2\right] + A_u^{\text{cue}}(t)\exp\left[-(\theta_H - \theta_{\text{cue},H}^{d,n})^2/2a_u^2\right] \quad (21)$$

In Fig. 3C and Fig. 4B, we fixed $\theta_{\text{cue}}^n = 20°$, $\theta_1^{n+1} = -30°$, and $\theta_2^{n+1} = 0°$. $A_u^{\text{cue}}(t)$, $A_u^1(t)$ and $A_u^2(t)$ decayed from the early delay period (Fig. S2D) to the late delay period (Fig. S2E). We calculated these parameters from the time point after S_2^{n+1} disappeared (t_0 = 7.8 s) to the time point before the cue period (t_e = 11.1 s), shown as dots in Fig. S2F, and found that they decayed exponentially with the time constant τ_f (curve in Fig. S2F), which can also be described as:

$$A_u^i(t) = A_u^i(t_0)\exp\left[-(t-t_0)/\tau_f\right], i = 1, 2, \text{cue} \quad (22)$$

where $A_u^{\text{cue}}(t_0) = 0.22$, $A_u^1(t_0) = 0.14$, $A_u^2(t_0) = 0.08$.

The above analysis is applicable to other combinations of θ_{cue}^n, θ_1^{n+1} and θ_2^{n+1}.

Table 5: The fitting parameters of u_H curve

t (s)	$\theta_{\text{cue}}^{d,n}$ (°)	$\theta_1^{s,n+1}$ (°)	$\theta_2^{s,n+1}$ (°)	A_u^{cue}	A_u^1	A_u^2	a_u
8.3	20.00	-30.00	0.00	0.20	0.12	0.07	0.31
10.8	20.00	-30.00	0.00	0.31	0.08	0.04	0.31

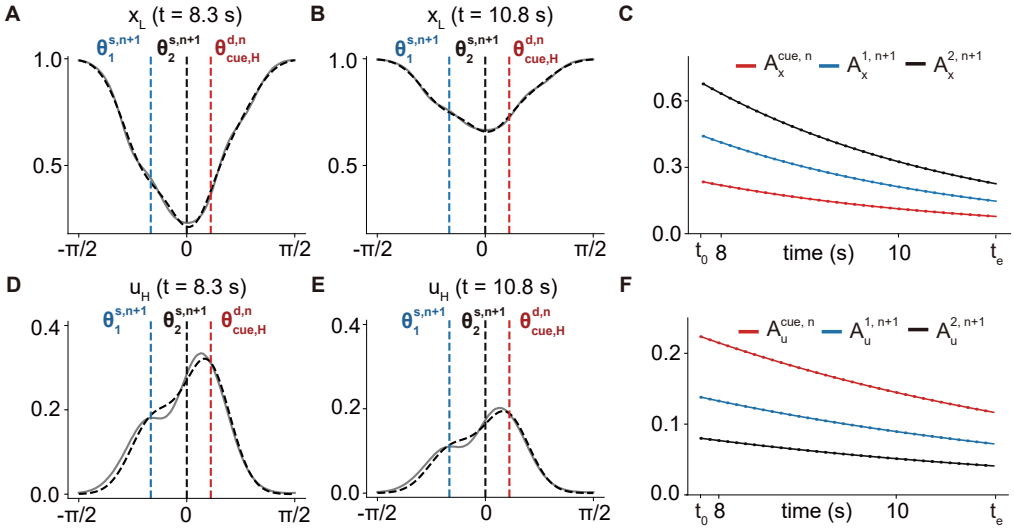

Figure S2: The fitting of x_L and u_H curves in a two-layer CANN. (A-C) x_L in an STD-dominated low layer. (D-F) u_H in an STF-dominated high layer.

D Dynamics of STP Variables

In Fig. 2A, we illustrated only the dynamics of the available neurotransmitter $x(\theta, t)$ to emphasize that, under the STD-dominated condition ($\tau_d \gg \tau_f$), the slow recovery of $x(\theta, t)$ is the main factor producing the repulsive effect. Here, the release probability $u(\theta, t)$ rapidly decays to zero after stimulus presentation and contributes minimally (Fig. S3A, top). Upon presentation of the retrieval signal, the instantaneous synaptic efficacy $u(\theta, t)x(\theta, t)$ shows an asymmetric distribution—the side near the previous stimulus S_1 is weaker (Fig. S3A, bottom), resulting in repulsion.

In Fig. 2D, we illustrated only the dynamics of the release probability $u(\theta, t)$ to highlight facilitation accumulation under the STF-dominated condition ($\tau_f \gg \tau_d$). Here, $x(\theta, t)$ rapidly recovers to baseline and contributes minimally (Fig. S3B, top). Upon retrieval, the synaptic efficacy $u(\theta, t)x(\theta, t)$ is enhanced near S_1 (Fig. S3B, bottom), producing an attractive bias.

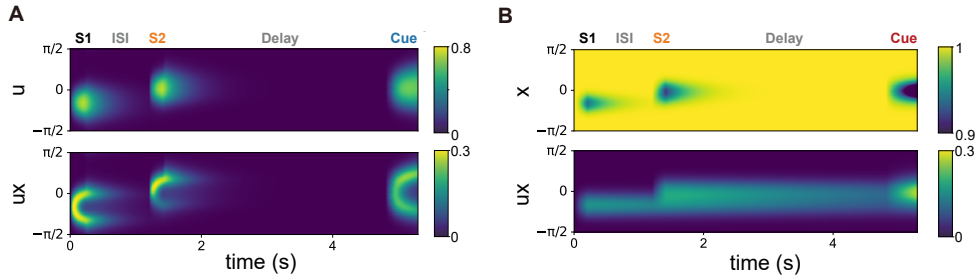

Figure S3: Dynamics of STP components in one-layer networks. (A) STD-dominated condition ($\tau_d \gg \tau_f$). Top: release probability $u(\theta, t)$ rapidly decays. Bottom: synaptic efficacy $u(\theta, t)x(\theta, t)$ is weaker near S_1. (B) STF-dominated condition ($\tau_f \gg \tau_d$). Top: available neurotransmitter $x(\theta, t)$ rapidly recovers. Bottom: synaptic efficacy $u(\theta, t)x(\theta, t)$ is enhanced near S_1.

E Control Analysis on the Recalled Stimulus in the Single-layer CANN

In the one-layer model (Fig. 2), only the second stimulus (S_2) was cued to examine the influence of the preceding one (S_1) on the subsequent one (S_2) based on the definition of *serial dependence*. To confirm that this choice does not qualitatively affect the model behavior, we conducted additional control experiments in which the one-layer model was re-run with random cueing of either S_1 or S_2 in interleaved trials.

The results showed that under STD-dominance, the model consistently exhibited a significant repulsive bias ($A_{\text{DoG}} = -3.51°$; $t(19) = 168.57$, $p < .001$, Fig. S4A), identical in sign and statistical significance to the repulsion reported in Fig. 2C. Under STF-dominance, the model consistently exhibited a significant attractive bias ($A_{\text{DoG}} = 1.68°$; $t(19) = 96.97$, $p < .001$, Fig. S4B), identical to the attraction reported in Fig. 2F. These findings demonstrate that the choice of the recalled stimulus (S_1 or S_2) does not alter the qualitative pattern of serial dependence, confirming the robustness of our main conclusions.

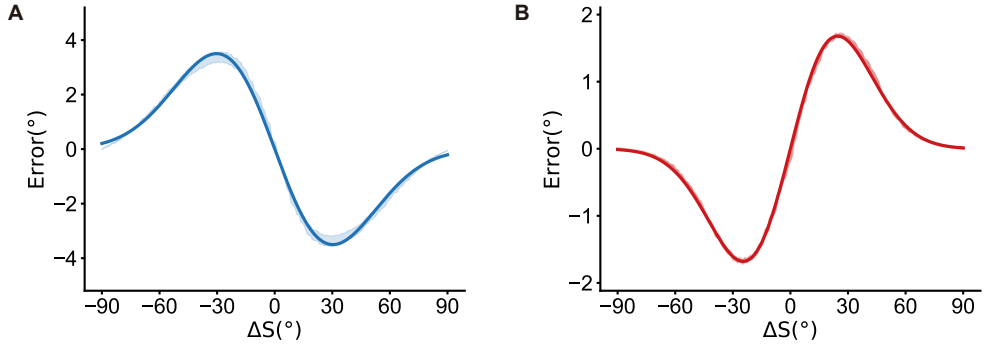

Figure S4: Control analysis of the recalled stimulus in the one-layer model. (A) STD-dominated single-layer CANN re-run with randomly cued S1 or S2 in interleaved trials. The adjustment error curve showed a significant repulsive bias. (B) STF-dominated single-layer CANN re-run with randomly cued S1 or S2 in interleaved trials. The adjustment error curve showed a significant attractive bias.

F Readout Rules

In our main analyses, we decoded orientation from neural activity via population vector method (PVM, Appendix A). To evaluate potential readout bias from asymmetrical responses, we reanalyzed Fig. 3D using three other methods:

Center-of-Mass (COM). The center-of-mass (COM) decoding computes the firing-rate-weighted circular mean of the population activity, implemented explicitly as a center-of-mass estimator on the

unit circle:

$$\hat{\theta}_{\mathrm{COM}} = \arg\left(\sum_i r_i e^{j\theta_i}\right).$$

In our simulations, the COM and population vector method (PVM) yield identical estimates. This equivalence arises because the tuning curves are symmetric, densely and uniformly distributed across the stimulus space, and without truncation or nonlinearity. Under such conditions, both COM and PVM effectively perform a linear weighted average of the population activity.

Maximum Likelihood (ML). We assume that each neuron's firing rate follows a Poisson distribution with a mean $\lambda_i(\theta)$ given by its tuning curve. The most likely stimulus $\hat{\theta}_{\mathrm{ML}}$ maximizes the log-likelihood function:

$$\hat{\theta}_{\mathrm{ML}} = \arg\max_{\theta} \sum_i \left[r_i \log \lambda_i(\theta) - \lambda_i(\theta) - \log(r_i!)\right].$$

We evaluated the log-likelihood across all candidate θ values and selected the one that yielded the maximum.

Peak Decoding (Peak). As a minimal heuristic, we also tested a peak decoder, which simply selects the preferred stimulus of the neuron with the highest firing rate:

$$\hat{\theta}_{\mathrm{Peak}} = \theta_{i^*}, \quad i^* = \arg\max_i r_i.$$

All three methods produced consistent results with PVM, confirming robust within-trial repulsion (serial bias amplitudes/curve peak at: PVM: -0.90°/37.92°, Fig. 3D; COM: -0.90°/37.92°, Fig. S5A; ML: -0.97°/36.97°, Fig. S5B; Peak: -0.61°/45.34°, Fig. S5C) and between-trial attraction (PVM: 1.17°/19.34°; COM: 1.17°/19.34°; ML: 1.05°/19.86°; Peak: 1.93°/18.21°). These results demonstrate that the qualitative pattern of serial dependence is robust to the choice of readout rule.

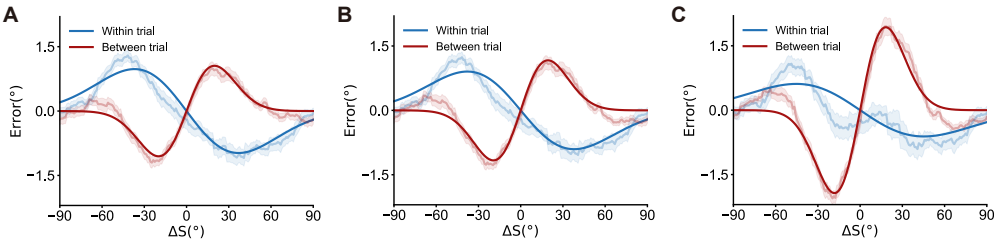

Figure S5: Comparison of different readout rules for decoding perceptual decisions. (A) Center-of-mass (COM) decoding. (B) Maximum likelihood (ML) decoding. (C) Peak decoding.

G Importance of the Order Between STD and STF Layers

To examine the importance of the order of short-term depression (STD) and short-term facilitation (STF) in the model architecture, we conducted control simulations with reversed synaptic configurations. A network with a lower STF-dominated layer ($\tau_f = 5$, $\tau_d = 0.3$) and a higher STD-dominated layer ($\tau_d = 3$, $\tau_f = 0.3$) exhibited exclusively attractive serial biases. Both within-trial effects and between-trial effects showed robust attraction (Fig. S6), confirming that the functional synergy between sensitivity and stability critically depends on the correct sequential order of STD and STF layers.

H Parameter Sensitivity Analysis

To evaluate the robustness of the model with respect to the choice of short-term plasticity (STP) parameters, we conducted a series of sensitivity analyses. The time constants for STD-dominated and STF-dominated synapses τs were selected based on previous physiological studies[47, 48, 53, 50] . As these parameters are critical for shaping the network dynamics, we varied their absolute values while preserving their dominance relationship (i.e., $\tau_d \gg \tau_f$ for STD, and $\tau_f \gg \tau_d$ for STF).

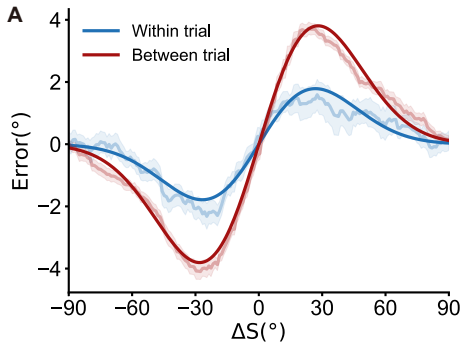

Figure S6: Effect of reversing STD/STF order on serial dependence bias. Both within-trial and between-trial bias curves showed exclusively attractive effects.

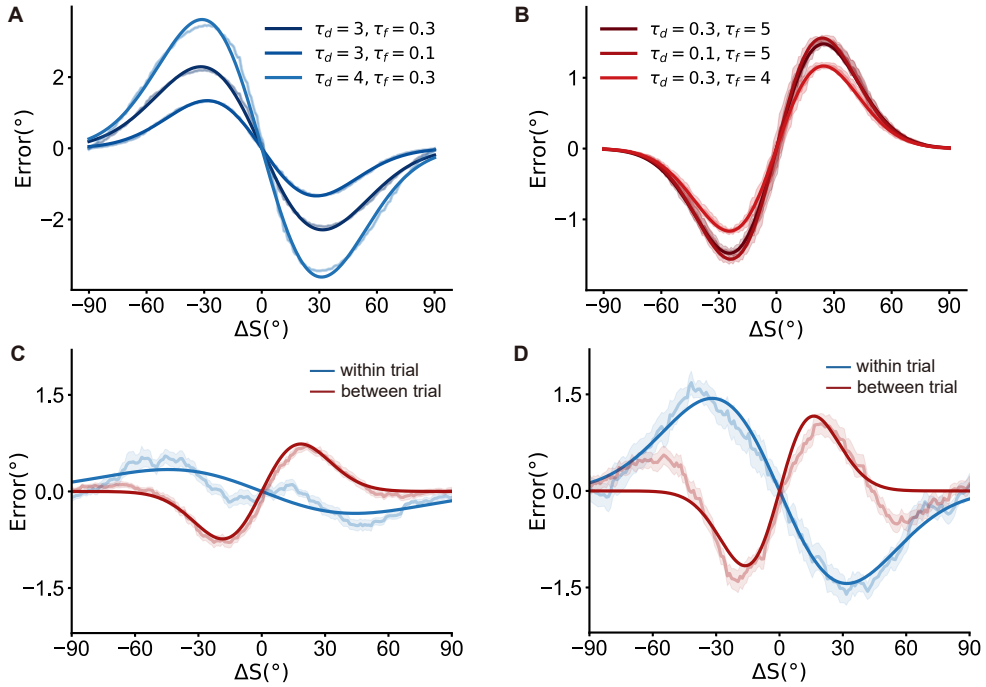

Figure S7: Sensitivity of serial dependence effects to short-term plasticity (STP) parameters. (A) Robustness of STD-dominated synapses in producing repulsive bias. All parameter sets showed significant repulsion effects. (B) Robustness of STF-dominated synapses in producing attractive bias. All parameter sets showed significant attraction effects. (C–D) Robustness of serial dependence in two-layer networks. In both cases, within-trial repulsion and between-trial attraction remained significant, differing only in effect magnitude.

Robustness of STD dominance in inducing repulsion effects. For the STD-dominated condition (Fig. 2C), we maintained $\tau_d \gg \tau_f$ and compared two sets of parameters ($\tau_f = 0.1$, $\tau_d = 3$ vs. $\tau_f = 0.3$, $\tau_d = 4$). In both cases, the model exhibited a statistically significant repulsion effect (both $t(19) > 213.97$, $p < .001$), with only the magnitude of repulsion varying ($-2.29°$ in Fig. 2C, $-1.34°$ and $-3.61°$ in Fig. S7A).

Robustness of STF dominance in inducing attraction effects. For the STF-dominated condition (Fig. 2F), we maintained $\tau_f \gg \tau_d$ and compared two sets of parameters ($\tau_f = 5$, $\tau_d = 0.1$ vs. $\tau_f = 4$, $\tau_d = 0.3$). In both cases, the model exhibited a statistically significant attraction effect (both $t(19) > 85.12$, $p < .001$), with only the magnitude of attraction varying ($1.48°$ in Fig. 2F, $1.56°$ and $1.16°$ in Fig. S7B).

Robustness of parameters in two-layer networks. Using the same ISI and ITI parameters as in Fig. 3D, we adjusted the absolute values of τ_d and τ_f in the low and high layers while preserving their relative relationships ($\tau_d^L \gg \tau_f^L$ and $\tau_f^H \gg \tau_d^H$). Serial dependence effects were computed for two parameter sets ($\tau_d^L = 2$, $\tau_f^H = 4$ in Fig. S7C; $\tau_d^L = 4$, $\tau_f^H = 6$ in Fig. S7D). The results showed that within-trial repulsion and between-trial attraction effects remained statistically significant (within-trial: both $t(19) > 5.52$, $p < .001$; between-trial: both $t(19) > 3.48$, $p < .01$), with only their magnitudes varying (within-trial: $-0.34°$ and $-1.44°$; between-trial: $0.73°$ and $1.16°$).

Our results demonstrated that, although changes in absolute values of τ_d and τ_f modulate the strength of sequence-dependent effects, it is their relative relationship (i.e., whether STD or STF dominance) that determines the qualitative nature of repulsion and attraction.

I Effect of Synaptic Heterogeneity on Model Performance

To explore how the heterogeneity of STP affects model performance, we re-ran the model with an inter-stimulus interval (ISI) of 1 s and applied $\pm 10\%$ random perturbations to STP parameters (τ_d and τ_f) of all synapses. Under STD-dominance, the adjustment error curve (variant STD, Fig. S8A) aligned with that in Fig. 2C (uniform STD, Fig. S8A). Results showed minimal amplitude change (from $-2.29°$ to $-2.28°$) and minimal DoG peak shift (from $31.71°$ to $31.78°$). Under STF-dominance, the adjustment error curve (variant STF, Fig. S8B) also closely matched that in Fig. 2F (uniform STF, Fig. S8B). Results showed stable attraction amplitude ($1.48°$) and minimal DoG peak shift (from $24.49°$ to $24.41°$). These results indicate that moderate heterogeneity in STP has a negligible impact on the qualitative pattern of serial dependence.

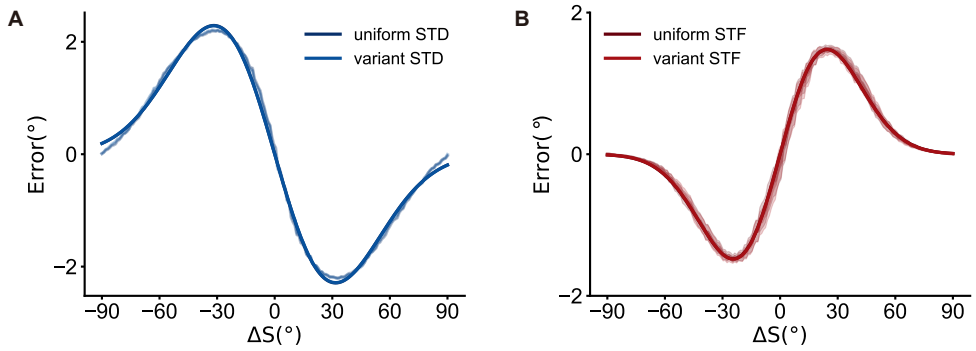

Figure S8: Effect of synaptic heterogeneity on model performance. (A) STD-dominated single-layer CANN re-run with uniform or variant τ_d. (B) STF-dominated single-layer CANN re-run with uniform or variant τ_f.